Aus dem Adolf-Butenandt-Institut – Lehrstuhl Molekularbiologie
im Biomedizinischen Centrum (BMC)
der Ludwig-Maximilians-Universität München
Vorstand: Univ.-Prof. Dr. rer. nat. Peter B. Becker

A NOVEL METHOD FOR FLUORESCENCE RECOVERY AFTER PHOTOBLEACHING (FRAP) ANALYSIS OF CHROMATIN PROTEINS IN PLURIPOTENT EMBRYONIC CELLS OF THE SOUTH AFRICAN CLAWED FROG *X. LAEVIS*

Dissertation
zum Erwerb des Doktorgrades der Medizin
an der Medizinischen Fakultät der
Ludwig-Maximilians-Universität München

vorgelegt von

Adrian Frhr. zu Innhausen u. Knyphausen

aus Bonn

2020

Mit Genehmigung der Medizinischen Fakultät
der Universität München

Berichterstatter:	Univ.-Prof. Dr. rer. nat. Ralph A. W. Rupp
Mitberichterstatter:	PD Dr. rer. nat. Christof Haffner Prof. Dr. med. Wolfgang E. Thasler
Dekan:	Univ.-Prof. Dr. med. dent. Reinhard Hickel
Tag der mündlichen Prüfung:	01. Oktober 2020

Eidesstattliche Versicherung

Ich erkläre hiermit an Eides statt, dass ich die vorliegende Dissertation mit dem Titel „**A novel method for Fluorescence Recovery after Photobleaching (FRAP) analysis of chromatin proteins in pluripotent embryonic cells of the South African clawed frog *X. laevis***“ selbstständig verfasst, mich außer der angegebenen keiner weiteren Hilfsmittel bedient und alle Erkenntnisse, die aus dem Schrifttum ganz oder annähernd übernommen sind, als solche kenntlich gemacht und nach ihrer Herkunft unter Bezeichnung der Fundstelle einzeln nachgewiesen habe.
Ich erkläre des Weiteren, dass die hier vorgelegte Dissertation nicht in gleicher oder in ähnlicher Form bei einer anderen Stelle zur Erlangung eines akademischen Grades eingereicht wurde.

Hamburg, den 01. Oktober 2020

Adrian Frhr. zu Innhausen u. Knyphausen

Meinen Eltern in Liebe und Dankbarkeit

Table of Contents

Das dieser Dissertation zugrunde liegende Forschungsprojekt wurde durch das *Förderprogramm für Forschung und Lehre (FöFoLe)* der Medizinischen Fakultät der Ludwig-Maximilians-Universität München sowie den *SFB 1064 – Chromatin Dynamics* gefördert.

Summary

This thesis describes a novel method for Fluorescence Recovery after Photobleaching (FRAP) analysis of chromatin proteins in pluripotent embryonic cells of the South African clawed frog *X. laevis*. This is the first application of this technique to nuclear proteins of native embryonic cells for this model organism.

An initial experiment made us aware that FRAP is not feasible for *Xenopus* embryos due to rapid movements of the cell nuclei, probably as a result of cytoplasmic streaming. However, an almost complete immobility of the structure to be investigated is a basic prerequisite for a successful FRAP experiment. Thus other experimental paths had to be explored at this point. In principle, three methodological approaches are conceivable to enable FRAP in *Xenopus*:

1. Cell nuclei are isolated from embryos or small embryonal dissections and attached to a microscopy slide by centrifugation. This method is already established but has conceptual shortcomings, as will be pointed out.
2. Embryos are used and efforts are made to reduce nuclear motion by inhibition of the molecular mechanisms underlying cytoplasmic streaming.
3. Cells are isolated from embryos or small embryonal dissections and nuclear motion is possibly reduced by adherence on a microscopy slide which is coated with a substrate yet to be found. It is conceivable that adherence leads to a change in the cell configuration in such a way that the range of motion of the cell nucleus within the cell is restricted and thus nuclear motion is reduced.

We considered it most promising to pursue the last option employing embryonic cells which have been isolated from animal caps, small dissections of pluripotent embryonic cells. We discovered that isolated animal cap cells adhere to a poly-L-lysine coated surface. This novel methodological approach leads to a sufficiently reduced nuclear motion for FRAP analyses.

The newly developed method was then used to characterize the two non-centromeric core histone H3 variants in *Xenopus*, H3.2 and H3.3, in pluripotent embryonic cells. The results obtained here contribute to a better understanding of the principles of core histone dynamics in early embryonic cells.

Zusammenfassung

Die vorliegende Arbeit beschreibt eine neuartige Methode für die Fluorescence Recovery after Photobleaching (FRAP)-Analyse von Chromatinproteinen in pluripotenten embryonalen Zellen des südafrikanischen Krallenfrosches *X. laevis*. Dies ist die erstmalige Anwendung dieser Technik auf nukleäre Proteine nativer embryonaler Zellen für diesen Modellorganismus.

Ein erstes Experiment führte uns vor Augen, dass FRAP an *Xenopus*-Embryonen aufgrund der schnellen Zellkernbewegungen, die am ehesten durch die zytoplasmatische Strömung bedingt sind, nicht möglich ist. Eine nahezu vollständige Immobilität der zu untersuchenden Struktur ist jedoch eine Grundvoraussetzung für ein gelingendes FRAP-Experiment. Daher müssen an diesem Punkt anderweitige experimentelle Pfade eingeschlagen werden. Im Prinzip sind drei methodische Ansätze vorstellbar, um FRAP an *Xenopus* zu ermöglichen:

1. Zellkerne werden aus Embryonen oder kleinen embryonalen Dissektaten vereinzelt und auf einen Objektträger durch Zentrifugation aufgebracht. Diese Methodik ist bereits etabliert, weist jedoch konzeptionelle Beschränkungen auf, auf die einzugehen sein wird.
2. Embryonen werden verwendet und es wird versucht, die Kernbewegung über eine Inhibition der der zytoplasmatischen Strömung zugrundeliegenden molekularen Mechanismen zu reduzieren.
3. Zellen werden aus Embryonen oder kleinen embryonalen Dissektaten vereinzelt und adhärieren möglicherweise auf einem Objektträger, der mit einem noch zu findenden Substrat beschichtet ist. Die Zelladhärenz führt dann möglicherweise zu einer Änderung der Zellkonfiguration in der Weise, dass der Bewegungsumfang des Zellkerns innerhalb der Zelle eingeschränkt und damit die Kernbewegung vermindert wird.

Wir hielten es für am vielversprechendsten, die letztgenannte Option weiterzuverfolgen und hierbei Animalkappen, kleine Dissektate pluripotenter embryonaler Zellen, zu verwenden. Wir stellten fest, dass Animalkappenzellen auf einer Poly-L-Lysin-beschichteten Oberfläche adhärieren. Dieser neuartige methodische Ansatz führt zu einer für FRAP-Analysen suffizient reduzierten Zellkernbewegung.

Die neu entwickelte Methode wurde dann dazu verwendet, die beiden nicht zentromerischen Core-Histon H3-Varianten in *Xenopus*, H3.2 und H3.3, in pluripotenten embryonalen Zellen zu charakterisieren. Die hier erzielten Ergebnisse tragen zu einem besseren Verständnis der Prinzipien von Core-Histon-Dynamik in frühen embryonalen Zellen bei.

1) Introduction

1.1) Chromatin plasticity and chromatin dynamics

Chromatin is the “molecular ensemble” of “genomic DNA together with all directly or indirectly associated protein and RNA molecules”. To name just a few examples, this includes histones, non-histone chromatin proteins and the transcription, replication and repair “machines” as well as mRNAs and lncRNAs (van Steensel, 2011).

Chromatin plasticity is the “diversity of properties for each cell type during development and also when cells face different environmental factors, genotoxic insults, metabolic changes, senescence, disease, and even death” (Yadav, Quivy and Almouzni, 2018; ➤ *Figure 1.1*). Hence, a plastic chromatin is a precondition for the capacity of the cell to adapt and for chromatin dynamics. Chromatin dynamics can be assessed by several approaches and techniques including, for instance, Fluorescence Recovery after Photobleaching (FRAP).

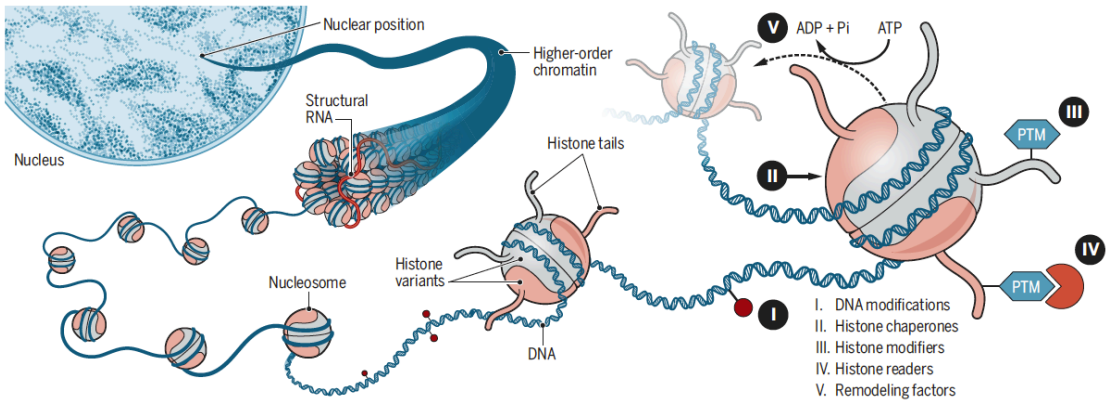

Figure 1.1: ***The molecular correlate of chromatin plasticity*** *(Yadav, Quivy and Almouzni, 2018)*

The set of properties of a given cell type at a given point of differentiation within given environmental conditions is specified by DNA modifications (I), ***histone variants*** *(➤ Chapter 1.1.2) and histone chaperones (II),* ***posttranslational modifications (PTMs) of histones*** *(➤ Chapter 1.1.3), histone modifiers (III), histone readers (IV) and ATP-dependent remodeling factors (V).*

1.1.1) Primary chromatin structure

Chromatin proteins are classified into a small group of histones on the one hand, and a large, heterogeneous group of non-histone chromatin proteins on the other hand. Histones are

subclassified into the four core histone groups (H2A, H2B, H3, H4) and one linker histone group (H1).

The core histones build up the nucleosome, the primary chromatin structure. The nucleosome assembles as follows: Two H3-H4 heterodimers build up a tetramer which is wrapped up by a ~70 bp DNA double strand. The nucleosome octamer is completed by association of two H2A-H2B heterodimers, around which another ~70 bp DNA-double strand is wrapped (Luger et al., 1997). Adjacent nucleosomes are linked by a 20-50 bp DNA double strand ("linker DNA"). Linker histones, which by definition are not part of the nucleosome, integrate into the linker DNA and thus stabilize the chromatin structure. Not every nucleosome is preceded by a linker histone. The ratio is slightly below 1.0 (van Holde, 1989) and even only ~0.5 in ES cells (Fan et al., 2003; Fan et al., 2005) (reviewed by Rupp and Becker, 2005).

Chromatin-associated RNA molecules comprise both coding RNA (mRNA) and non-coding RNA (long (>200 nucleotides) non-coding RNA (lncRNA)). lncRNAs are assumed to represent a "molecular trafficking system" for the recruitment of chromatin modifiers within cellular programs such as X-inactivation or imprinting (Koziol and Rinn, 2010; Hung and Chang, 2010).

1.1.2) Histone variants

1.1.2.1) Classification

Each histone group, with the exception of the H4 group, includes several histone variants which differ, to varying degrees, in base pair sequence, number of (non-allelic) genes, protein structure, post-translational modifications, time of deposition, chaperones and, last but not least, function.
Some variants are deposited to DNA exclusively within S-phase (replication-dependent), others are deposited to chromatin independently from the cell cycle (replication-independent). The replication-dependent variants are encoded by highly repetitive, "canonical" genes, organized in clusters, whereas the replication-independent variants are encoded by a few singular, "non-canonical" genes (Zink and Hake, 2016; Buschbeck and Hake, 2017; Talbert and Henikoff, 2017).
Deposition/eviction of histone variants into/from chromatin is governed by chaperones, protein complexes with the capacity for ATP-dependent chromatin remodeling. Sitbon et al. (2017) shaped the simplified but not inaccurate picture of histone variants as the "bricks" and chaperones as the "architects".

1.1.2.2) Histone H3 variants in *X. laevis*

The histone H3 group in *X. laevis* includes the replication-dependent, canonical variant H3.2, the replication-independent, non-canonical variant H3.3, as well as the centromere-specific, replication-dependent variant cenH3 (CENP-A) (Hake and Allis, 2006). Unlike mammals, *X. laevis* has only one replication-dependent H3 variant and thus, the individual contribution of a replication-dependent variant on the one hand, and a replication-independent variant on the other hand, to a given phenotype can be directly correlated (Sitbon et al., 2017). The genes or gene clusters coding for the H3 variants in *X. laevis* are listed in the following table.

Histone H3 variant	Gene* / Gene cluster*
H3.2 (canonical)	h3.2a (hist1h3g, hist2h3)
H3.3 (non-canonical)	h3f3a (h3.3, h3.3a) h3f3b (h3.3b)
cenH3 (CENP-A)	cenp-a (cenpa)

* *according to xenbase.org*

We use murine H3.2 and H3.3 in this work, both highly conserved between *X. laevis* and *M. musculus*: as for H3.3, the amino acid sequence is identical (➤ *Figure 1.3*), as for H3.2, the amino acid sequences differ in one amino acid or one methyl-group (glycine instead of alanine at position 112) (➤ *Figure 1.2*). The amino acid sequences of mammalian H3.2 and H3.3 differ in four amino acids.

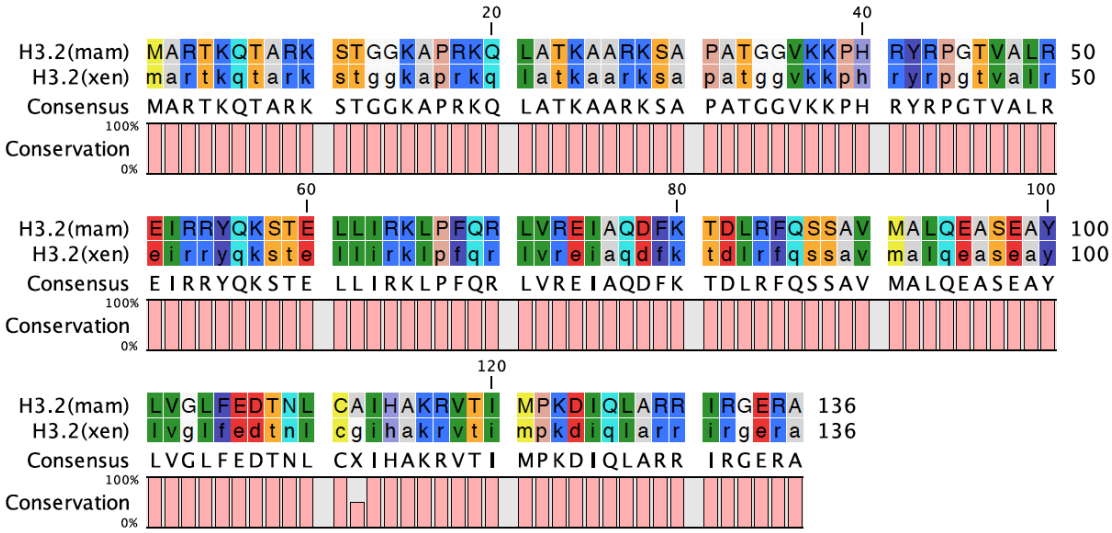

Figure 1.2: ***H3.2 amino acid sequence alignment: mammalian (mam) vs. X. laevis (xen) H3.2*** *(by CLC sequence viewer)*

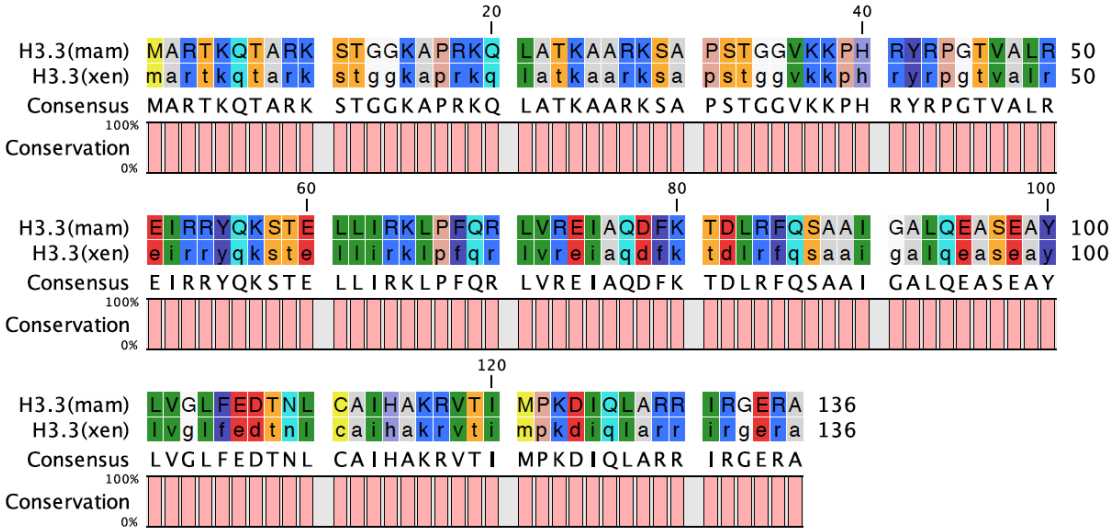

Figure 1.3: ***H3.3 amino acid sequence alignment: mammalian (mam) vs. X. laevis (xen) H3.3*** *(by CLC sequence viewer)*

1.1.2.3) Histone H3 chaperones

The histone H3 variants are deposited into/evicted from chromatin in dimerization with H4 by dedicated chaperones (➤ *Figure 1.4*).

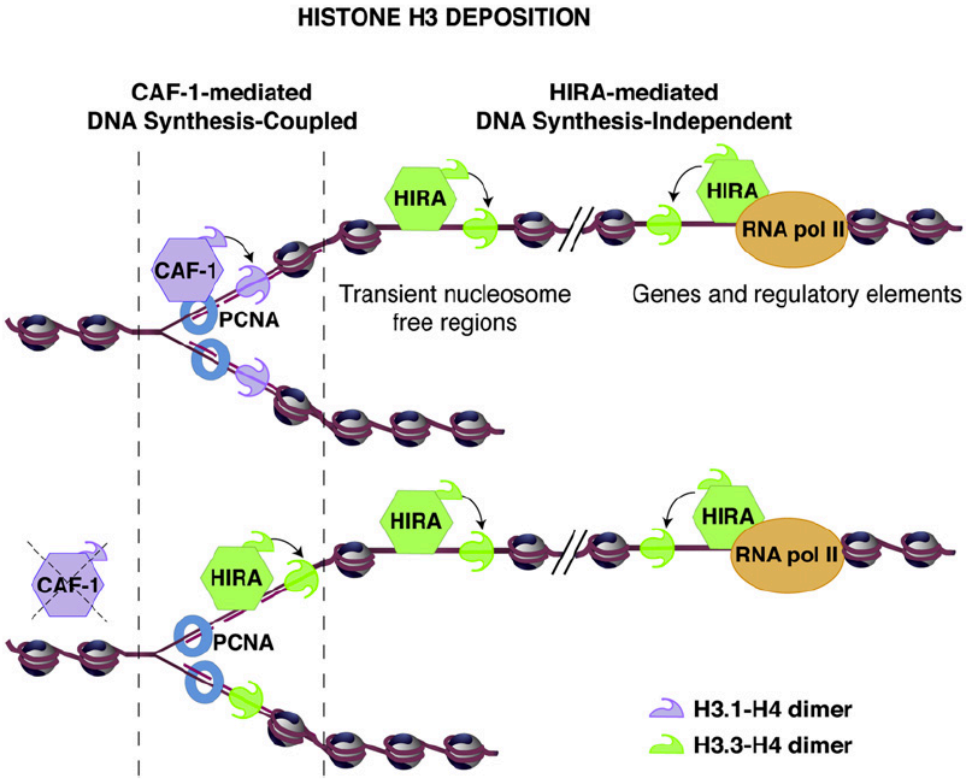

***Figure 1.4:* Differential chromatin deposition of histone H3 variants by dedicated chaperones** *(Ray-Gallet et al., 2011)*

The replication-dependent variants H3.1 and H3.2 are deposited to newly replicated, "naked" DNA in a random, non-selective manner by the chaperone complex CAF-1 (chromatin assembly factor 1) (Tagami et al., 2004).

The deposition of the replication-independent variant H3.3 is more complex: H3.3 is deposited to sites of active gene transcription by HIRA (Ray-Gallet et al., 2002; Tagami et al., 2004; Ricketts et al., 2015; Ray-Gallet et al., 2018), although not exclusively, as deposition to a number of transcription factor binding sites is HIRA-independent (Goldberg et al., 2010). Also, H3.3 is deposited by the same chaperone in a non-selective manner to "naked" DNA after DNA double-strand break repair (Li and Tyler, 2016). In the case that the deposition of H3.1/H3.2 is halted due to inhibition of CAF-1, H3.3 is exceptionally deposited to newly replicated DNA by HIRA and thus, partially compensates for the absence of H3.1/H3.2 (Ray-Gallet et al., 2011).

And finally, H3.3 is deposited to repetitive heterochromatin by DAXX (death-domain associated protein) which is in complex with the ATP-dependent chromatin remodeler ATRX. This includes retrotransposons, pericentric heterochromatin and telomers. Specific mutations in ATRX cause the alpha-thalassemia, mental retardation, X-linked syndrome (for which it was named) as well as several adult and pediatric tumors (Drané et al., 2010; Goldberg et al., 2010; Lewis et al., 2010; reviewed in Dyer et al., 2017).

Thus, on the one hand, H3.3 is enriched at sites of active transcription, but on the other hand, H3.3 localizes as well to repetitive heterochromatic regions, reflecting the "double" or "Janus face" of H3.3 (Szenker et al., 2011).

1.1.2.4) Excursion: H3.3 and its role as a prominent "oncohistone"

According to a conservative estimate, about 4% of all tumors have a mutation in one of the core histones, although we are only just beginning to understand the prevalence and significance of "oncohistones" (Nacev et al., 2019).

For example, mutations in one of the two non-allelic genes for H3.3 (H3F3A and H3F3B), occasionally combined with a mutation in DAXX/ATRX, have been identified in several malignant brain, bone and cartilage tumors. *Figure 1.5* provides an overview of all neoplasia-linked mutations in H3F3A and H3F3B identified so far. Notably, the H3.3K27M and H3.3G34R/V alterations have been the first alterations within the amino acid sequence of a core histone which could be linked to a malignant tumor (pediatric glioblastoma multiforme) (Schwartzentruber et al., 2012).

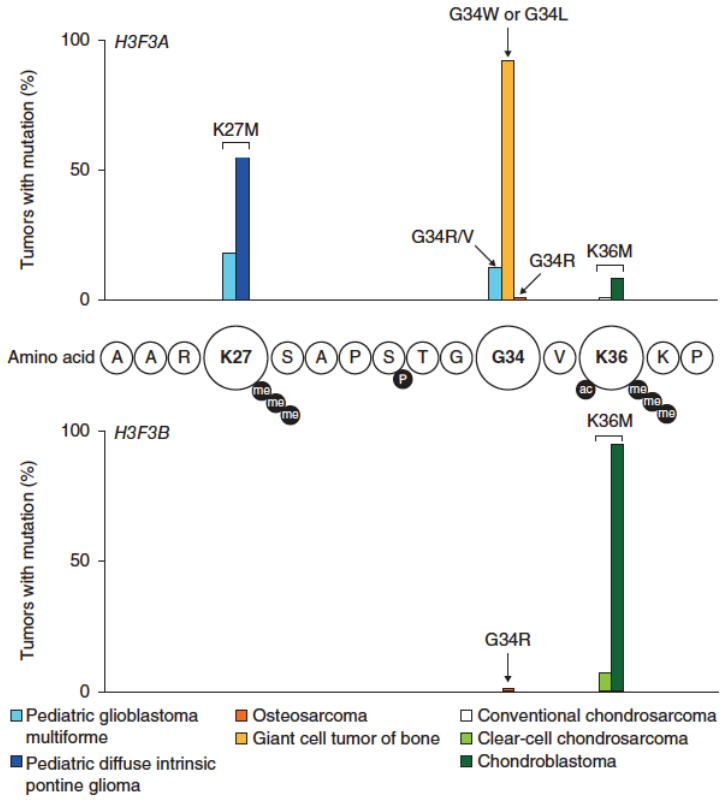

Figure 1.5: ***Neoplasia-associated mutations in H3F3A and H3F3B*** *(Behjati et al., 2013)*
95% of chondroblastoma have a H3.3K36M alteration, encoded in first line by H3F3B (93%) and in second line by H3F3A (7%). Furthermore, 92% of giant cell tumor of bone have a H3.3G34W/L alteration, encoded exclusively by H3F3A.
With regard to malignant brain tumors, 71% of pediatric diffuse intrinsic pontine glioma and 20% of pediatric glioblastoma multiforme show a H3.3K27M alteration, exclusively encoded by H3F3A. 10% of pediatric glioblastoma multiforme alternatively have a H3.3G34R/V alteration, all of them additionally mutated in DAXX/ATRX. 7% of pediatric diffuse intrinsic pontine glioma with a H3.3K27M mutation additionally have an ATRX mutation (Behjati et al., 2013; Khunong-Quang et al., 2012; Schwartzentruber et al., 2012).

1.1.3) Posttranslational histone modifications

All core histones can be posttranslationally diversified by chemical groups or small polypeptides on specific amino acid residues, preferably on the N-terminal histone tail. These posttranslational modifications (PTMs) are reversible. They include, but are by far not limited to, methylation, acetylation, SUMOylation, ubiquitination and ribosylation of lysine residues, as well as phosphorylation of serine and threonine residues (Cheung, Allis and Sassone-Corsi, 2000; Jenuwein and Allis, 2001; Bhaumik et al., 2007; Kouzarides, 2007).

In addition to histone variants, PTMs represent another molecular basis of chromatin plasticity. PTMs interfere with virtually all cellular programs such as, to give just a few examples, transcription, replication and DNA-repair, as well as chromatin condensation and segregation (MacAlpine and Almouzni, 2013; Yadav, Quivy and Almouzni, 2018). PTMs fundamentally regulate the accessibility of genes for enhancer and other regulatory elements by direct (chromatin structure) and indirect (recruitment of chromatin remodelers) mechanisms.

1.1.4) Higher order chromatin structure

The chromatin structure beyond the nucleosome is not fully unraveled yet, however, both for the secondary and the tertiary chromatin structure, partly complementary, partly competing models exist. In particular, the decoding of the secondary chromatin structure poses a challenge due to methodological limitations (Risca and Greenleaf, 2015). The next figure provides an orientating view of the current idea of higher order chromatin structure.

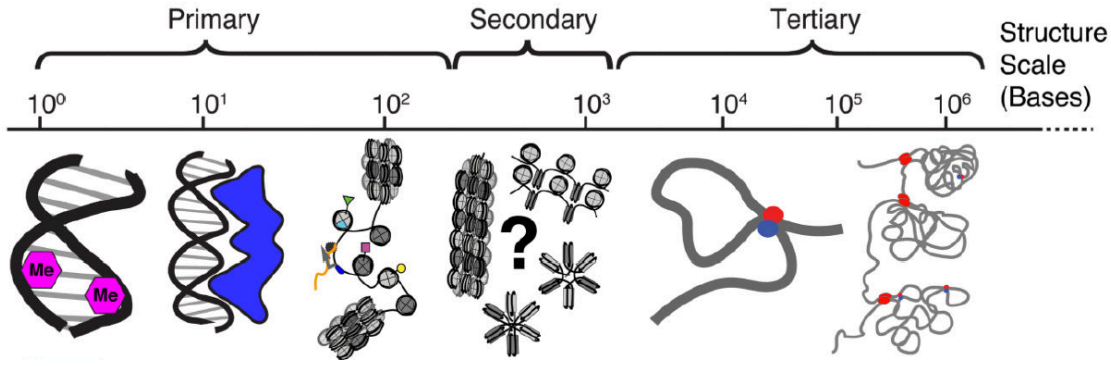

***Figure 1.6:* Primary and higher order chromatin structure** *(Risca and Greenleaf, 2015)*
The primary chromatin structure is the nucleosome, neighboring nucleosomes are connected by linker DNA, into which linker histones are scattered at irregular intervals. So far, it is assumed, that the secondary chromatin structure is defined, possibly beside other mechanisms yet to be identified, by nucleosome-nucleosome interactions which themselves are determined by DNA methylation (pink), DNA binding factors (DBFs, blue), histone variants and PTMs (multicolored). The tertiary chromatin structure has been recognized to be defined by DNA(red)-protein on DNA(blue)-loops across several to several hundreds of kilobases as well as by DNA(red)-DNA(red)-loops at megabase scale, even if possible further mechanisms could play a role here.

1.2) Dissecting chromatin dynamics by Fluorescence Recovery after Photobleaching (FRAP)

Fluorescence Recovery after Photobleaching (FRAP) is a technique among the kinetic microscopy techniques (the "F-techniques": FRAP, FLIP, FCS and others) which combine *in vivo* imaging and kinetic modelling approaches. These techniques allow one to analyze dynamic processes within the cell, the nucleus and other cell organelles such as mitochondria or the Golgi complex (Phair and Misteli, 2001; Lippincott-Schwartz et al., 2018).
A FRAP experiment follows always the same course: Fluorescent (macro)molecules are irreversibly photobleached in a small area by an intense laser beam and the subsequent fluorescence recovery is recorded by the same but attenuated laser beam. Fluorescence recovery is the diffusion of fluorescent molecules from the non-bleached into the bleached area, which can then be specified with the aid of a kinetic model to be selected.

The first application of FRAP (at that time Fluorescence photobleaching recovery, FPR) was reported by Axelrod et al. in 1976: A small spot within a thin aqueous layer of the fluorescent molecule rhodamine 6G had been bleached and, perhaps more importantly, a first kinetic model had been developed (see also Axelrod et al. 2018, a reminiscence on the "classic" FRAP article in 1976).
The first cloning of the fluorophore of the jellyfish Aequorea victoria ("GFP") (Prasher et al., 1992), the first expression of GFP in a eukaryotic organism (Caenorhabditis elegans) (Chalfie et al., 1994), the development of the enhanced variant eGFP (Heim, Cubitt and Tsien, 1995) (O. Shimomura, M. Chalfie and R. Tsien, Nobel Prize in Chemistry 2008) as well as the advancement of confocal and *in vivo* microscopy has led to a renaissance of the FRAP technique in the mid-nineties (Misteli and Spector, 1997).
Golgi membrane proteins were initially investigated by FRAP (Cole et al., 1996; Presley et al., 1997), nuclear and chromatin proteins followed soon after (Phair and Misteli, 2000; Misteli et al., 2000).

A molecule is fluorescent either by autofluorescence (*fluorophores*, e.g. rhodamine 6G, GFP, eGFP) or by coupling to a fluorophore. Each fluorophore contains a small subdomain called the *chromophore*, a conjugated π-electron resonance system which is the functional unit of fluorescence. For instance, eGFP has a p-hydroxybenzylideneimidazolinone chromophore which results from cyclization, dehydrogenation and oxidation of a short 3-aa-sequence (Thr65 – Tyr66 – Gly67) (Cubitt et al., 1995). The electrons within the conjugated π-electron resonance system are first excited by energy in the form of light at a distinct wavelength, before the electrons lose energy in the form of light at a distinct wavelength ("fluorescence"). This physical process is visualized by the Jablonski diagram (➤ *Figure 1.7*).

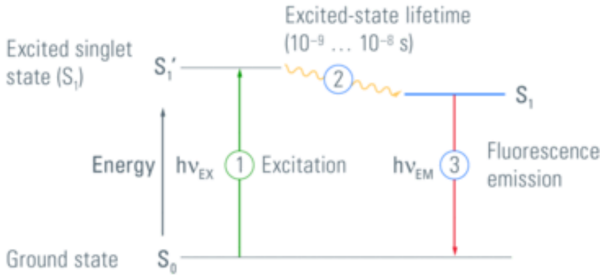

***Figure 1.7:* Jablonski diagram (Greb, 2012)**

Electrons within a chromophore are excited by energy in the form of light at a defined wavelength, the energy level is lifted from ground state S_0 to the excited singlet state S_1' (excitation (1)). Once excited, electrons constantly lose energy, the energy level decreases from S_1' to S_1. After 10^{-9}-10^{-8} s (excited state lifetime (2)), electrons abruptly lose the remaining energy in the form of light at a defined wavelength, the energy level returns to ground state S_0 (fluorescence emission (3)). The wavelength of the emitted light is longer than the wavelength of the exciting light (Stoke's shift).

An electron cannot be excited indefinitely: Upon a certain number of excitation cycles, the chromophore becomes irreversibly non-functional. The chromophore can be rendered non-functional (i.e. the fluorescence is "bleached") either by a sufficiently long or a sufficiently high-energetic electron excitation.

1.3) Pluripotent embryonic cells in *X. laevis*

The South African clawed frog *Xenopus laevis* (Daudin, 1802) has repeatedly and substantially contributed to our understanding of (embryonic) development, developmental epigenetics, pluripotency and reprogramming to pluripotency by nuclear transfer (nuclear transfer embryonic stem cells (NT-ES cells)) (J. Gurdon and S. Yamanaka, Nobel Prize in Physiology or Medicine 2012).

This model organism has some outstanding qualities, two of which are pointed out here: First, the embryos are grown in a simple, additive-free saline solution. And second, the embryonic development is extrauterine and (pluripotent) embryonic cells can be dissected directly from the embryo (animal caps, see below) and can be used without further treatment.

Animal caps are small dissections from the animal pole of the blastula embryo. Depending on time of dissection, animal cap cells represent either totipotency (early blastula, NF8, 5-7 hpf at 23°C) or pluripotency (late blastula, NF9, 7-9 hpf at 23°C). Animal caps have been repeatedly used in the fields of inductive differentiation and *in vitro* organogenesis (exemplary Okabayashi and Asashima, 2006).

Murine embryonic stem cells (mES cells) – the standard model for pluripotency

A number of pluripotent embryonic cells cultured *in vitro* can be differentiated in mammals. "Classic" embryonic stem cells (ES cells) derive from the inner cell mass (embryoblast) of the blastocyst. Along with embryo implantation, the inner cell mass differentiates into a hypoblast part and an epiblast part, from which the three germ layers develop. Another embryonic stem cell type can be derived from this epiblast part, the so-called epiblast stem cells (epiSCs). At least in Germany, this type of stem cell derivation is currently restricted to rodents for ethical reasons.

Both ES cells and epiSCs do not represent the "genuine" pluripotency of the original cells. Rather, the ES cells are ascribed a so-called "naive" pluripotency, the epiSCs a so-called "primed" pluripotency. These two “shades of pluripotency” are then further graduated depending on the culture medium used (➤ *Figure 1.8*). The individual culture media shift the pluripotency to a more naive or a more primed state (Weinberger et al., 2016).

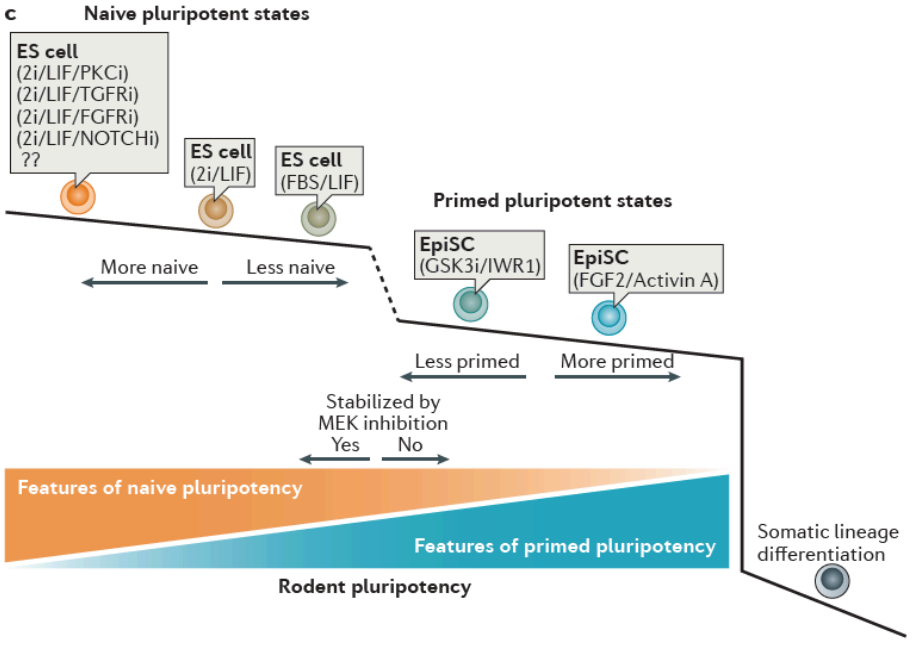

***Figure 1.8:* Graduation of naive and primed pluripotency depending on the culture medium used** *(Weinberger et al., 2016)*

“Naive pluripotency” is attributed to ES cells which derive from the inner cell mass of the blastocyst, “primed pluripotency” is ascribed to epiSCs which originate from the epiblast part of the post-implantation embryo. The distinction between these two “shades of pluripotency” can be made upon the effect of inhibition of the mitogen-activated protein kinase kinase (MEK) by a kinase inhibitor.

Both serum-supplemented (FBS (fetal bovine serum)) and serum-free media (2i, 3i) are used for the cultivation of ES cells and epiSCs. Serum-free media differ in number and composition of small molecule kinase inhibitors and growth factors. The use of a FBS-containing medium shifts pluripotency towards a more primed state.

In summary, pluripotent embryonic stem cells have no direct counterpart *in vivo* (Surani et al., 2007) and the “shade of pluripotency” depends on the culture medium used.

1.4) Current application of FRAP to *X. laevis*

FRAP has already been applied in various ways to *X. laevis*, for example to oocytes to characterize the diffusion properties of maternal mRNAs (Powrie et al., 2016; Ciocanel et al., 2017). Moreover, Eroshkin et al. (2016) compared the diffusion characteristics of Noggin proteins within the intercellular space on embryos at gastrula stage, as well as Higashi et al. (2016), who characterized the diffusion kinetics of tight junctions and adherens junctions proteins of the interphase cell membrane, as well as of the M-phase cleavage furrow and polar region.

However, nuclear or chromatin protein dynamics in native embryonic cells have not been analyzed so far. The underlying methodological difficulties are illustrated in Aoki et al (2010): The nuclei are described here as “dark and poorly outlined due to yolk-rich cytoplasm” and to be “in motion as a result of protoplasmic streaming” (see below). To bypass these problems, Aoki et al. developed a so-called “*in vitro* reconstitution system” (see below) which enables the assessment of chromatin protein mobility in cell nuclei isolated from embryonic cells.

Protoplasmic streaming

Protoplasmic streaming, cytoplasmic streaming or cyclosis has been first described for plant cells by B. Corti already in 1774 and is defined as continuous and directed motility of the cytoplasm that enables transportation of biomolecules and cell organelles. Cytoplasmic streaming has since been detected in a number of plant and metazoan cells and has been found to be associated with cytoskeleton-based intracellular transport processes. The cytoskeleton is a proteinaceous meshwork of actin and intermediate filaments as well as microtubules, along which cargo-carrying motorproteins, including myosin (on actin filaments), dynein and kinesin (both on microtubules), “walk” in a characteristic manner under ATP-hydrolysis. These motorproteins bind and transport vesicles, organelles and biomacromolecules, to name just a few.

The actomyosin complex generates local hydrodynamic flows which align neighboring actin filaments. In this way, large-scale hydrodynamic flows, i.e. cytoplasmic streaming, is generated (Ueda et al., 2010; Woodhouse and Goldstein, 2012; Woodhouse and Goldstein, 2013). The same mechanism applies to kinesin motorproteins on microtubules (Serbus et al., 2005), but is complicated by mechanical interactions between microtubules (Suzuki et al., 2017).

Cytoplasmic streaming is particularly relevant for the accelerated transport of biomolecules over long intracellular distances in order to maintain the metabolic rate. This explains why

cyclosis is regularly found in exceptionally large cells. Since embryonic *Xenopus* cells are also unusually large (30-50 µm at mid-blastula, Williams et al., 2004), a pronounced cytoplasmic streaming can be assumed here. In addition, the remarkably consistent size of eukaryotic cells in the range of 1-100 µm could be related to cytoplasmic streaming: About 100 µm seems to be the maximum distance over which timely transportation by cytoplasmic streaming is practicable (Goldstein and van de Meent, 2015).

The "*in vitro* reconstitution system" by Aoki et al.

This experimental setup allows the assessment of chromatin protein mobility in cell nuclei isolated from embryonic cells. This method proceeds as follows: Nuclei are isolated mechanically and cytoplasm is "extracted" enzymatically from embryos or embryonal dissections at various developmental stages. The nuclei and cytoplasmic extracts are then recombined in all possible combinations. The nuclei are attached to a glass slide by centrifugation. The measured fluorescence recoveries for H1 and HP1 are continuously up to 50% below the values acquired in established systems. Thus, this is a method for the "assessment" of chromatin protein mobility, as the authors themselves say; however, the precise measurement of protein mobilities is not sufficiently achieved by this method.

1.5) Objectives

As pointed out in *Chapter 1.3*, (pluripotent) embryonic *Xenopus* cells have at least two major advantages compared to ES cells and are therefore particularly suited for chromatin characterization by FRAP and comparable techniques:

1. Pluripotent embryonic *Xenopus* cells can be dissected directly from the embryo and can be used without further treatment. Hence, these cells represent genuine *in vivo* pluripotency.
2. Pluripotent embryonic *Xenopus* cells are cultured in simple, additive-free saline solution and thus, genuine pluripotency is maintained.

Therefore, it is a worthwhile goal to implement FRAP on (pluripotent) embryonic *Xenopus* cells. The experimental work is structured into two parts:

1. **Implementing FRAP on embryonic *Xenopus* cells**
   The cell nuclear motion described above could be a challenge.
2. **Analyzing chromatin dynamics in embryonic *Xenopus* cells by FRAP**
   We decided for H3.2 and H3.3, as these H3 variants are in an interesting interplay. In addition, FRAP analyses for these proteins have already been conducted in established systems.

2) Materials and Methods

2.1) Special laboratory equipment

Device	Company
ChemiDoc™ Touch Imaging System	Bio-Rad, Hercules, CA, USA
Confocal Laser Scanning Microscope Leica TCS SP5 II	Leica, Wetzlar, Germany
Microscope Temperature Control System "The Cube & The Box"	Live Imaging Services, Basel, Switzerland
Incubator Heracell™ 240i	Thermo Fisher Scientific, Waltham, MA, USA
Incubator HettCube 400 R	Hettich, Tuttlingen, Germany
Micropipette Puller P-87	Sutter Instrument, Novato, CA, USA
Picoliter Microinjector PLI-100A	Warner Instruments, Hamden, CT, USA
Spectrophotometer DS-11	DeNovix, Wilmington, DE, USA
Ultracentrifuge Optima™ MAX-XP	Beckman Coulter, Krefeld, Germany

2.2) Molecular biology methods

2.2.1) Gateway™ cloning

DNA templates for murine H3.2-eGFP and H3.3-eGFP have been kindly provided by S. B. Hake (now *University of Gießen*, Germany) and have been cloned into a pCS2+GW-vector using the Gateway™ technique (Invitrogen, Carlsbad, CA, USA).
In a first step, the DNA-templates are amplified by PCR. In view of the subsequent cloning of these templates into a donor vector exhibiting a specific recombinant sequence (*attP*), primers with a specific recombinant sequence (*attB*) are used (see following table).

Primer	5' → 3' sequence
attB1_H3.2 (for) (enzyme: XhoI)	GGGGACAAGTTTGTACAAAAAAGCAGGCTTAACTATGGCG CGTACTAAGCAGACGGCTC
attB2_H3.2 (rev)	GGGGACCACTTTGTACAAGAAAGCTGGGTCCGCCCTCTCCC CACGAATGC
attB1_H3.3 (for) (enzyme: XhoI)	GGGGACAAGTTTGTACAAAAAAGCAGGCTTAACTATGGCCC GAACCAAGCAGAC
attB2_H3.3 (rev)	GGGGACCACTTTGTACAAGAAAGCTGGGTCAGCTCTCTCTC CCCGTATCCG

The PCR was then run using the following protocols.

PCR	Amount, Concentration	Volume
ddH_2O		to 100 µl
Advantage® 2 PCR Buffer*	10 x	10 µl
DNA template	320 ng	
dNTP Mix	10 mM each	2 µl
Primer (for) (attB1)		2 µl
Primer (rev) (attB2)		2 µl
Advantage® 2 Polymerase Mix*	50 x	2 µl

* Clontech, Mountain View, CA, USA

Thermocycling Step	Temperature	Time	Cycles
Denaturation	94°C	2 min	1 x
Denaturation	94°C	15 s	
Annealing	58°C*	30 s	{ 30 x
Elongation	68°C	30 s**	
Elongation	68°C	7 min	1 x
Cooling	4°C	∞	

** The annealing temperature depends on the GC content of the primers. The primer-specific melting temperature Tm is calculated with the "NEB Tm Calculator" (tmcalculator.neb.com).*

*** The elongation time depends on the size of the gene to be amplified.*

In a second step, the now amplified and *attB*-flanked DNA-templates are cloned into a donor vector by BP Clonase™ II (BP reaction, see following table). The product is the entry clone with a recombinant *attL* sequence.

BP reaction	Amount	Volume
TE buffer		to 4 µl
attB-flanked DNA template	150 ng	
Donor vector	150 ng	1 µl
BP Clonase™ II*		1 µl

* Invitrogen, Carlsbad, CA, USA

In a third step, the *attL*-flanked DNA template within the entry clone is cloned into a pCS2+GW-vector (destination vector) by LR Clonase™ (LR reaction, see following table). The end product is the expression clone.

LR reaction	Amount	Volume
TE buffer		to 4 µl
attL-flanked DNA template (within the entry clone)	150 ng	
Destination vector	150 ng	1 µl
LR Clonase™*		1 µl

* Invitrogen, Carlsbad, CA, USA

2.2.2) Plasmid linearization

Prior to the *in vitro* transcription, the DNA plasmids first have to be linearized.

Reagent	Amount, Concentration	Volume
ddH_2O		to 40 µl
Buffer B*	10 x	4 µl
DNA plasmid	10 µg	
Asp718 I*	10 U/µl	3 µl

* Roche, Basel, Switzerland

2.2.3) *In vitro* transcription

The *in vitro* transcription was conducted according to the following protocol.

Reagent	Amount, Concentration	Volume
DEPC H_2O		to 50 µl
Transcription buffer*	5 x	10 µl
Linearized plasmid	2 µg	
NTP mix**	10 mM each	5 µl
Cap analog***	25 mM	5 µl
DTT*	100 mM	5 µl
RNAsin*	40 U/µl	0.5 µl
SP6 RNA Polymerase*	20 U/µl	2 µl
Incubation at 37°C for 2.5 h		
SP6 RNA Polymerase*	20 U/µl	1 µl
Incubation at 37°C for 1 h		
DNAse I*	10 U/µl	1 µl
*Incubation at 37°C for 0.5 h and mRNA clean up (RNeasy Mini Kit****)*		

* Promega, Madison, WI, USA

** Roche, Basel, Switzerland

*** NEB, Ipswich, MA, USA

**** Qiagen, Venlo, Netherlands

2.2.4) Cell transfection

A6 cells have been plated at a density of 2 x 10^4 cells/well in the four central wells of an 8 well µ-slide® (ibidi, Martinsried, Germany) about 24 hours prior to the transfection. The composition of the transfection complex is given in the following table.

Reagent	Amount per well
1. DMEM* (w/o serum)	30 µl
2. Plasmid DNA	0.3 µg
3. X-tremeGENE™ HP DNA Transfection Reagent**	0.3 µl (1:1 DNA-to-reagent ratio)

* Sigma-Aldrich, St. Louis, MO, USA

** Roche, Basel, Switzerland

The transfection complex first rests at room temperature for 15 minutes and then is trickled onto the cells. The FRAP experiments were conducted with a latency of 24 hours.

2.2.5) Western-blot

Biologicals and Chemicals	Company
Glycine	VWR, Radnor, PA, USA
Immobilon™ Western	Merck Millipore, Burlington, MA, USA
SDS 20%	Serva, Heidelberg, Germany
TWEEN® 20	Sigma-Aldrich, St. Louis, MO, USA

Buffers	Component	Amount, Conc.
TBS-T(WEEN® 20)	NaCl	150 mM
	TRIS	50 mM
	TWEEN® 20	0.05%
	HCl	to pH 7.4

10 x Running buffer	TRIS	30.2 g
	Glycine	188 g
	SDS 20%	50 ml
10 x Blotting buffer	TRIS	30.2 g
	Glycine	188 g
	1 x dilution: 70% ddH_2O, 10% 10 x blotting buffer, 20% MeOH	

Primary antibodies				
Antigen	**Dilution**	**Species**	**Company**	**Catalog #**
GFP	1:10,000	Mouse	Roche, Basel, Switzerland	11814460001
panH3	1:20,000	Rabbit	Abcam, Cambridge, UK	ab1791
Secondary antibodies				
Antigen	**Dilution**	**Species**	**Company**	**Catalog #**
Mouse	1:10,000	Sheep	VWR, Radnor, PA, USA	NA931
Rabbit	1:10,000	Donkey	VWR, Radnor, PA, USA	NA934

2.3) Tissue culture

Cell lines	**Company**
A6 cells (26°C, 5% CO_2)	American Type Culture Collection (ATCC), Manassas, VA, USA
HeLaK cells (37°C, 5% CO_2)	S. B. Hake (now *University of Gießen*, Germany)

Biologicals	**Company**
Dulbecco's Modified Eagle's Medium (DMEM) – high glucose	Sigma-Aldrich, St. Louis, MO, USA
Fetal calf serum (FCS)	Sigma-Aldrich, St. Louis, MO, USA
Geneticin (G418)	Sigma-Aldrich, St. Louis, MO, USA
Penicillin, Streptomycin (P/S)	Life Technologies, Carlsbad, CA, USA
Poly-L-lysine solution (0.1%)	Sigma-Aldrich, St. Louis, MO, USA

Culture media	Component	Concentration
DMEM 90% (HeLaK)	DMEM	90%
	FCS	10%
	P/S	1%
	G418	1%
DMEM 75% (A6)	DMEM	75%
	ddH_2O	15%
	FCS	10%
	P/S	1%

2.4) *X. laevis*-specific methods and techniques

2.4.1) Cultivation

Biologicals and Chemicals	Company
Cysteine hydrochloride 1-hydrate	AppliChem, Darmstadt, Germany
Gentamicin	Sigma-Aldrich, St. Louis, MO, USA

Culture media	Component	Amount
10 x MBS (Modified Barth's saline)	NaCl	880 mM
	KCl	10 mM
	$MgSO_4$	10 mM
	HEPES	50 mM
	$NaHCO_3$	25 mM
	NaOH	to pH 7.8
	$CaCl_2$ is added to 0.1 x MBS. The $CaCl_2$-concentration in 0.1 x MBS is 0.7 mM.	
10 x Steinberg's solution, Ca^{2+}- and Mg^{2+}-free, EDTA-supplemented (SS w/o)	NaCl	580 mM
	KCl	6.7 mM
	HEPES	50 mM
	EDTA	0.1 mM
	HCl	to pH 7.34-7.44

X. laevis embryos have been grown in gentamicin-supplemented (0.1%) MBS (0.1 x) at 23°C. The developmental staging has been made according to the *Normal Table of Xenopus laevis (Daudin)* by Nieuwkoop and Faber (1994).

***In vitro* fertilization**

Eggs are obtained by gentle squeezing of β-HCG-ovulated females and collected in a Petri dish. A small piece of testis is fragmented within a few milliliters of 1 x MBS. The sperm suspension is then trickled onto the eggs which rest for about 10 minutes before the dish is filled with 0.1 x MBS.

Removal of the jelly coat

Eggs and embryos are engulfed by a jelly coat, which is a protective barrier to chemical absorption (Edginton et al., 2007). Embryos are transferred into an Erlenmeyer flask which is filled with cysteine-supplemented (2%) MBS (0.1 x). The flask is carefully swiveled until the jelly coat is detached after approx. 5 minutes. The embryos are then rinsed several times to remove any remaining cysteine.

2.4.2) Micromanipulation techniques

Microinjection

Microneedles are made from glass tubes (Glass 1BBL W/FIL 1.0 mm, World Precision Instruments, Sarasota, FL, USA) by a micropipette puller (settings: Heat: 800, Pull: 35, Velocity: 140, Time: 139). The pulled end of the microneedle is broken back manually by tweezers to achieve delivery of approx. 5 nl-drops under defined microinjector settings (pressure: 30 psi, time: 40 ms). The final drop size is fine-tuned over the injection time. In case of higher deviations, the microneedle is discarded.

Animal cap dissection

Animal caps are dissected using two pairs of tweezers (Biology No. 5) (Dumont, Montignez, Switzerland). The embryo is first “unpacked” by stripping of the vitelline membrane. One tip of the first tweezers is then pierced into the embryo, 0.2-0.5 cm distant from the center of the animal pole. The pair of tweezers is closed and a second pair of tweezers detaches the tissue held by the first tweezers. This procedure is repeated several times until the animal cap is completely explanted.

2.4.3) Cell nuclei isolation and chromatin extraction

Biologicals and Chemicals	Company
cOmplete™ Protease Inhibitor Cocktail (tablets)	Roche, Basel, Switzerland
DTT	Biomol, Hamburg, Germany
Glycerol	VWR, Radnor, PA, USA
NP-40	Honeywell, Morris Plains, NJ, USA

Buffers	Component	Amount, Conc.
C complete	NaCl	420 mM
	$MgCl_2$	2 mM
	HEPES / KOH pH 7.9	20 mM
	Glycerol	20 Vol.-%
	Added immediately before use:	
	DTT	0.5 mM
	cOmplete™	1 tablet
	NP-40	0.1%
E1 complete w/o sucrose (B4)	KCl	90 mM
	$MgCl_2$	5 mM
	TRIS / HCl pH 7.4	50 mM
	EDTA	0.1 mM
	Added immediately before use:	
	DTT	2 mM
	cOmplete™	1 tablet
E1 complete + 0.25 M sucrose (B1)	E1 complete	50 ml
	Sucrose	4.3 g
E1 complete + 1.25 M sucrose (B3)	E1 complete	50 ml
	Sucrose	21.6 g
E1 complete + 0.25 M sucrose + 0.2% NP-40 (B2)	E1 complete	50 ml
	Sucrose	4.3 g
	Added immediately before use:	
	NP-40	0.1 ml

Cell nuclei isolation

Nuclei have been isolated from blastula embryos applying the protocol of Schneider et al. (2011). The first steps are carried out at room temperature. About 100 embryos are transferred into a 1.5 ml-Eppendorf tube, filled with 1 ml B1 buffer. B1 is exchanged three times, always preceded by a centrifugation at 600 rpm for 1 min. Finally, the embryos rest in B1 for 20 min. Then the embryos are transferred into a glass tissue homogenizer (S) (Braun, Melsungen, Germany) after two more milliliters of B1 have been added. The embryos are lysed by 10 slow and gentle pushes. The embryo suspension is transferred into a 15 ml-Falcon tube and centrifuged at 1,000 rpm for 10 min at 4°C. From this step on, all the following are carried out at 4°C. The pellet is resuspended in 3 ml B2, the suspension rests 20 min, is transferred into a 50 ml-Falcon tube, filled with 5 ml B3, and centrifuged at 1,000 rpm for 30 min. The supernatant ("sucrose supernatant") is subjected to a protein precipitation according to Wessel and Flügge (1984), the pellet is resuspended in 1.5 ml B4. The suspension is transferred into a 1.5 ml-Eppendorf tube which is centrifuged at 5,000 rpm for 2 min. The supernatant is discarded and the pellet, isolated nuclei, is submitted to the next step of chromatin extraction.

Chromatin extraction

Chromatin and histones, respectively, can be extracted from isolated cell nuclei by two methods, *acid extraction* and *high salt extraction* (reviewed in Shechter et al., 2007). The fact that histones can be purified relatively easily by acid extraction due to their basic character was already described in 1884 by Albrecht Kossel, the first describer of histones (A. Kossel, Nobel Prize in Physiology or Medicine 1910). The acid extraction in this work was conducted according to the protocol by H. Christian Eberl.

Like the final steps of cell nuclei isolation, chromatin extraction is performed at 4°C. The nuclei isolation pellet is twice resuspended in 10 ml PBS and the suspension is centrifuged at 3,900 rpm for 5 min. The pellet is resuspended in 3 ml C complete, the suspension is rotated for 1 h and ultracentrifuged at 55,000 rpm for 1 h. The ultracentrifugation pellet ("UZ pellet") is pure chromatin and the ultracentrifugation supernatant ("UZ supernatant") is chromatin-free extract. The UZ supernatant is subjected to a Wessel and Flügge-protein precipitation.

2.4.4) Poly-L-lysine coating of µ-slides®

We used 8 well µ-slides® (ibidi, Martinsried, Germany) for FRAP microscopy. These polymeric slides are refined by a standard tissue culture coating (ibiTreat®). To enable adhesion of animal cap cells, we added a poly-L-lysine coating according to the ibidi Application Note No. 8 (Coating procedures for ibidi µ-slides and µ-dishes). The positively charged polyamino acid poly-l-lysine enhances electrostatic interaction between the net negatively charged cell surface and the positively charged slide surface.

300 µl of diluted poly-L-lysine solution (15 µg/ml) are pipetted into each of the four central wells. The slide rests at room temperature for 1 hour before the solution is removed and each well is rinsed five times with 300 µl 1 x PBS. After the final PBS removal, the slide is kept in a vertical position for at least half an hour to allow even drying.

2.5) Technical aspects of FRAP measurements

2.5.1) Data acquisition

The microscope settings used for FRAP measurements are listed in the following table.

Parameter	Setting
AOTF	
- pre- and postbleach image recording (488 nm)	2%
- bleaching (all lines)	100%
Bidirectional scan	✓
Binary digit (bit)	12 bit
Diameter of the bleached ROI (px)	40 px
Format	256 x 256 px
Frames (prebleach, bleaching, postbleach)	
- HeLaK cells	20, 2, 391
- A6 cells	20, 5, 391
- animal cap cells	20, 5, 196
Laser	Argon laser
Laser power	100%
Laser lines	
- pre- and postbleach image recording	488 nm
- bleaching	458 nm, 476 nm, 488 nm, 514 nm
Pinhole aperture	2 AU
Postbleach image recording time	
- HeLaK cells, A6 cells	60 s
- animal cap cells	30 s
Scan speed	870 Hz
Smart gain	800 V
Zoom	
- HeLaK cells, A6 cells	10 (except for eGFP (Zoom 8))
- animal cap cells	8

Zoom in	*X*
Pixel size (depending on Zoom) - *Zoom 8* - *Zoom 10*	 *120.6 x 120.6 nm* *96.48 x 96.48 nm*
Diameter of the bleached ROI (µm) (depending on number of pixels (40 px, see above) and pixel size) - *120.6 x 120.6 nm* - *96.48 x 96.48 nm*	 *4.824 µm* *3.859 µm*
Time / frame (depending on scan speed and bidirectional scan)	 *0.154 s*
Temperature ("The Cube & The Box")	23°C

2.5.2) Data evaluation

Primary data analysis

In a first step, the FRAP stack is imported into an R-macro which converts image data into numerical data. In each individual frame, a numerical value is assigned to the fluorescence intensity in the three regions of interest (➤ *Figure 2.1*). This R-macro has been developed in cooperation with Kathrin Schneider (Leonhardt group, *LMU*) and has been specially designed for our microscope. The entire script is provided in Appendix III.

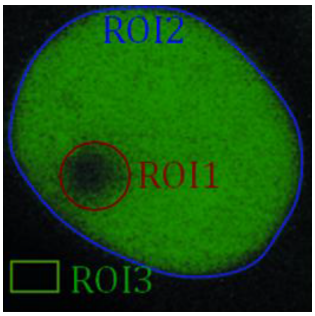

***Figure 2.1:* Regions of interest (ROIs) (Rapsomaniki et al., 2012)**

ROI1: bleached area

ROI2: non-bleached area (here: non-bleached area of the nucleus)

ROI3: background (here: cytoplasm)

Secondary data analysis

In a second step, the Excel file with the fluorescence intensity values for the three regions of interest is imported into easyFRAP, an open-access, non-commercial software (Rapsomaniki et al., 2012). In the following, the individual processing steps of this software are presented.

Background subtraction

The background fluorescence intensity (*ROI3*) is subtracted from the fluorescence intensity in *ROI1* and *ROI2*, respectively.

$$I(t)_{ROI1'} = I(t)_{ROI1} - I(t)_{ROI3}$$

$$I(t)_{ROI2'} = I(t)_{ROI2} - I(t)_{ROI3}$$

Bleaching depth

Bleaching depth (bd), a measure for the bleaching efficacy, is the spread between the mean prebleach fluorescence intensity I_I (non-normalized) and the first postbleach fluorescence intensity I_α (non-normalized) in *ROI1*.

$$Bd = \frac{\left(\frac{1}{n_{pre}} \cdot \sum_{t=1}^{n_{pre}} I(t)_{ROI1'}\right) - I(t_{bleach})_{ROI1'}}{\frac{1}{n_{pre}} \cdot \sum_{t=1}^{n_{pre}} I(t)_{ROI1'}}$$

Gap ratio

Gap ratio (gr), a measure for the loss of fluorescence intensity in the non-bleached area during postbleach time, is the spread between the mean prebleach fluorescence intensity I_I (non-normalized) and the mean postbleach fluorescence intensity (non-normalized) in *ROI2*. A high gap ratio means a small loss of fluorescence intensity.

$$Gr = \frac{\frac{1}{10} \cdot \sum_{t_{bleach}}^{t_{bleach}+10\Delta t} I(t)_{ROI2'}}{\frac{1}{n_{pre}} \cdot \sum_{t=1}^{n_{pre}} I(t)_{ROI2'}}$$

Double normalization

easyFRAP offers a double normalization and a full-scale normalization. Both types of normalization correct the gap ratio (first part of the equation). A full-scale normalization additionally corrects the bleaching depth. We decided for a double normalization.

$$I(t)_{norm}^{double} = \left(\frac{\frac{1}{n_{pre}} \cdot \sum_{t=1}^{n_{pre}} I(t)_{ROI2'}}{I(t)_{ROI2'}} \right) \cdot \left(\frac{I(t)_{ROI1'}}{\frac{1}{n_{pre}} \cdot \sum_{t=1}^{n_{pre}} I(t)_{ROI1'}} \right)$$

Bi-exponential fit

easyFRAP provides a mono-exponential ("single term") and a bi-exponential ("double term") fit. We tested both fits and decided on the basis of R^2 for the bi-exponential fit.

$$I_{fit2} = I_0 - ae^{-\beta t} - \gamma e^{-\delta t}$$

Mobility fractions

Mobility fractions indicate the ratio of the soluble or loosely bound and the non-soluble, i.e. bound fraction of molecules of a given protein. The soluble fraction is indicated by the mobile fraction, the non-soluble fraction by the immobile fraction.

The mobile fraction is the spread between the endpoint fluorescence intensity I_∞ (normalized) and the first postbleach fluorescence intensity I_α (normalized). The immobile fraction is the spread between the mean prebleach fluorescence intensity I_I (normalized, hence $I_I = 1$) and the endpoint fluorescence intensity I_∞ (normalized).

$$Mf = \frac{I_\infty - I_a}{1 - I_a}$$

$$if = 1 - mf$$

t-half (t/2)

t/2 specifies the time at which the postbleach fluorescence intensity has recovered to 50% of the mean prebleach fluorescence intensity I_I. t/2 is calculated numerically.

Coefficient of determination R^2

The coefficient of determination R^2 is a measure for the goodness of the mathematical fit. An equation that perfectly fits the data predicts the dependent variable y at each x ($R^2 = 1$). An equation that does not fit the data at all cannot predict y ($R^2 = 0$).

3) Results

3.1) Establishing the FRAP technique

Before we started to work on methodological details of the application of FRAP to embryonic *Xenopus* cells, we first had to establish this technique in our laboratory. Besides learning the practical handling of the confocal microscope, the initial focus was on selecting appropriate programs for primary and secondary data analysis or, if necessary, developing new ones. As described in *Chapter 2.5.2*, we use a self-developed R-macro for primary data analysis and an open-access software for secondary data analysis (easyFRAP).

In the course of my first two experimental series, FRAP data were to be reproduced on the locally available confocal microscope and using the selected analysis programs. To this end, we repeated in parts the FRAP analyses of Wiedemann et al. (2010), who characterized the then newly identified primate-specific histone variants H3.X and H3.Y in HeLaK cells, among other methods also by FRAP analysis. The FRAP experiments in Wiedemann et al. were conducted under the guidance of L. Schermelleh (now *Advanced Bioimaging Unit*, *University of Oxford*, UK). We selected a completely soluble, highly mobile protein (eGFP) and a mainly non-soluble, virtually immobile protein (eGFP-H3.3) to cover the entire range of protein mobility. Moreover, we adopted the microscope settings from Wiedemann et al.. The results of the FRAP analyses for these two proteins on stably transfected HeLaK cells are presented in the following two figures.

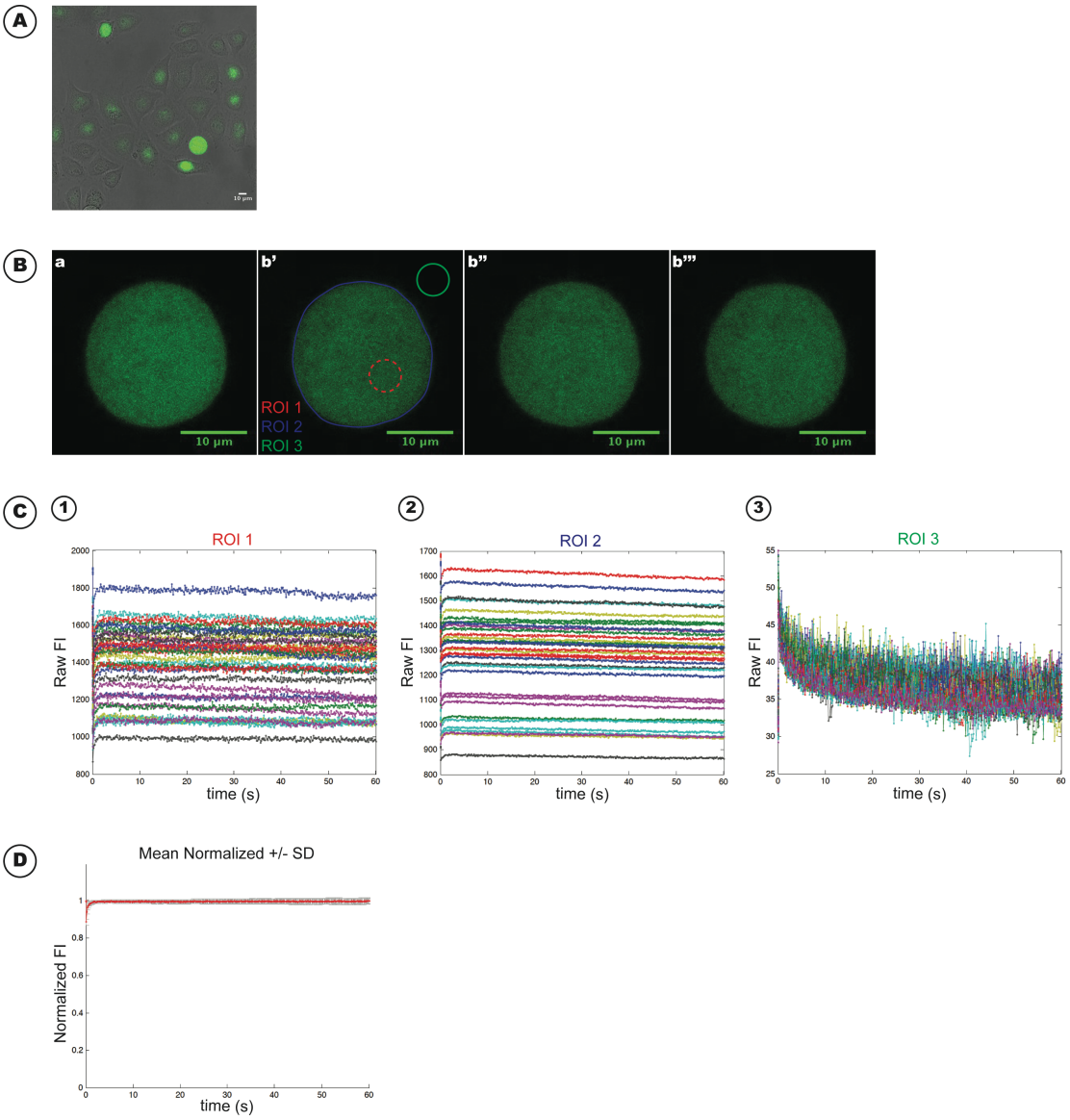

***Figure 3.1:* FRAP analysis for eGFP in HeLaK cells**

*(**A**) Cell morphology (brightfield + GFP, scale bar: 10 µm). Completely soluble eGFP is distributed in the entire cytoplasm.*

*(**B**) Selected frames (scale bar: 10 µm) (**a**) prebleach (**b'**) postbleach 1 (0.154 s) (**b''**) postbleach 2 (30 s) (**b'''**) postbleach 3 (60 s)*

*(**C**) Fluorescence Intensity (FI) in (**1**) ROI1 (**2**) ROI2 (**3**) ROI3 for individual cell measurements (arbitrary units) • Bleaching Depth: 81% • Gap Ratio: 94%*

*(**D**) Mean normalized curves +/- SD • t/2: 0.17 s • Mobile Fraction: 100% • R^2: 59%*

n = 33 cells from 3 independent experiments

The bleaching event was effective, as can be read from the bleaching depth. Even before the first postbleach frame was taken, the initial concentration of eGFP in the bleached area was restored. eGFP is highly mobile as indicated by the mobile fraction and by t/2. Half of the mean initial fluorescence intensity of a completely soluble protein is recovered within 0,17 s.

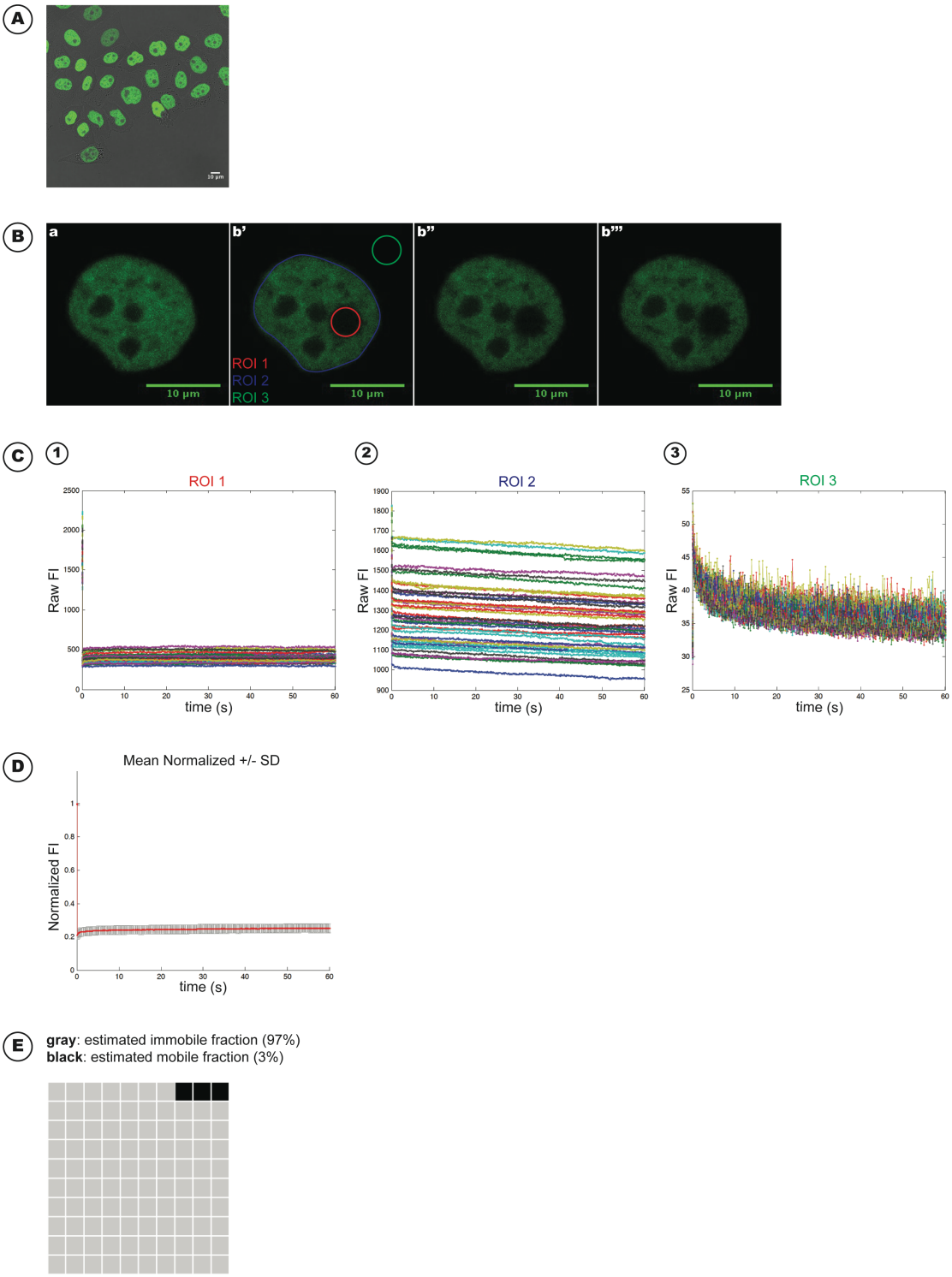

***Figure 3.2:* FRAP analysis for eGFP-H3.3 in HeLaK cells**

*(**A**) Cell and nuclear morphology (brightfield + GFP, scale bar: 10 µm)*

*(**B**) Selected frames (scale bar: 10 µm) (**a**) prebleach (**b'**) postbleach 1 (0.154 s) (**b''**) postbleach 2 (30 s) (**b'''**) postbleach 3 (60 s)*

*(**C**) Fluorescence Intensity (FI) in (**1**) ROI1 (**2**) ROI2 (**3**) ROI3 for individual cell measurements (arbitrary units) • Bleaching Depth: 81% • Gap Ratio: 90%*

*(**D**) Mean normalized curves +/- SD • t/2: not calculable* • R^2: 98%*

*(**E**) Mobility Fractions (waffle chart)*
n = 42 cells from 3 independent experiments
The vast majority of eGFP-H3.3 molecules are non-soluble, as indicated by the immobile fraction of 97%.
** t/2 cannot be calculated because the fluorescence intensity in the selected postbleach time does not reach 50% of the mean prebleach fluorescence intensity. We will encounter a t/2 that is not predictable for this reason also in the following experiments (*).*

These first two studies confirm that we can reproduce published FRAP data with our equipment. The microscope settings and the obtained values for bleaching depth and gap ratio serve as reference settings and reference values, respectively, for the following FRAP analyses. Accordingly, the bleaching depth should be around 80%, the gap ratio around 90%.

3.2) FRAP analyses for H3.2 and H3.3 in epithelial *Xenopus* cells (A6 cells)

The next step was to apply FRAP to epithelial *Xenopus* cells. To this end, we selected the A6 cell line which has been derived from the kidney of an adult male *X. laevis* frog (Rafferty, 1969). The transient transfection of the A6 cells with expression plasmids for eGFP-tagged histone variants was performed as described in *Chapter 2.2.4*.
We used the reference microscope settings and found that the bleaching depth, unlike the gap ratio, is significantly below the reference level. The bleaching depth can be regulated by the laser power, the used laser lines for bleaching, the permeability of the AOTF filters during bleaching and the bleaching time. Since the first three parameters were already set at maximal levels, the bleaching depth could only be improved by the bleaching time. We extended the bleaching time from 308 ms to 770 ms and reached bleaching depths of 80% and 81%, respectively. With these modified settings, FRAP analyses have now been made for H3.2-eGFP and H3.3-eGFP, the results of which are shown in the next two figures.

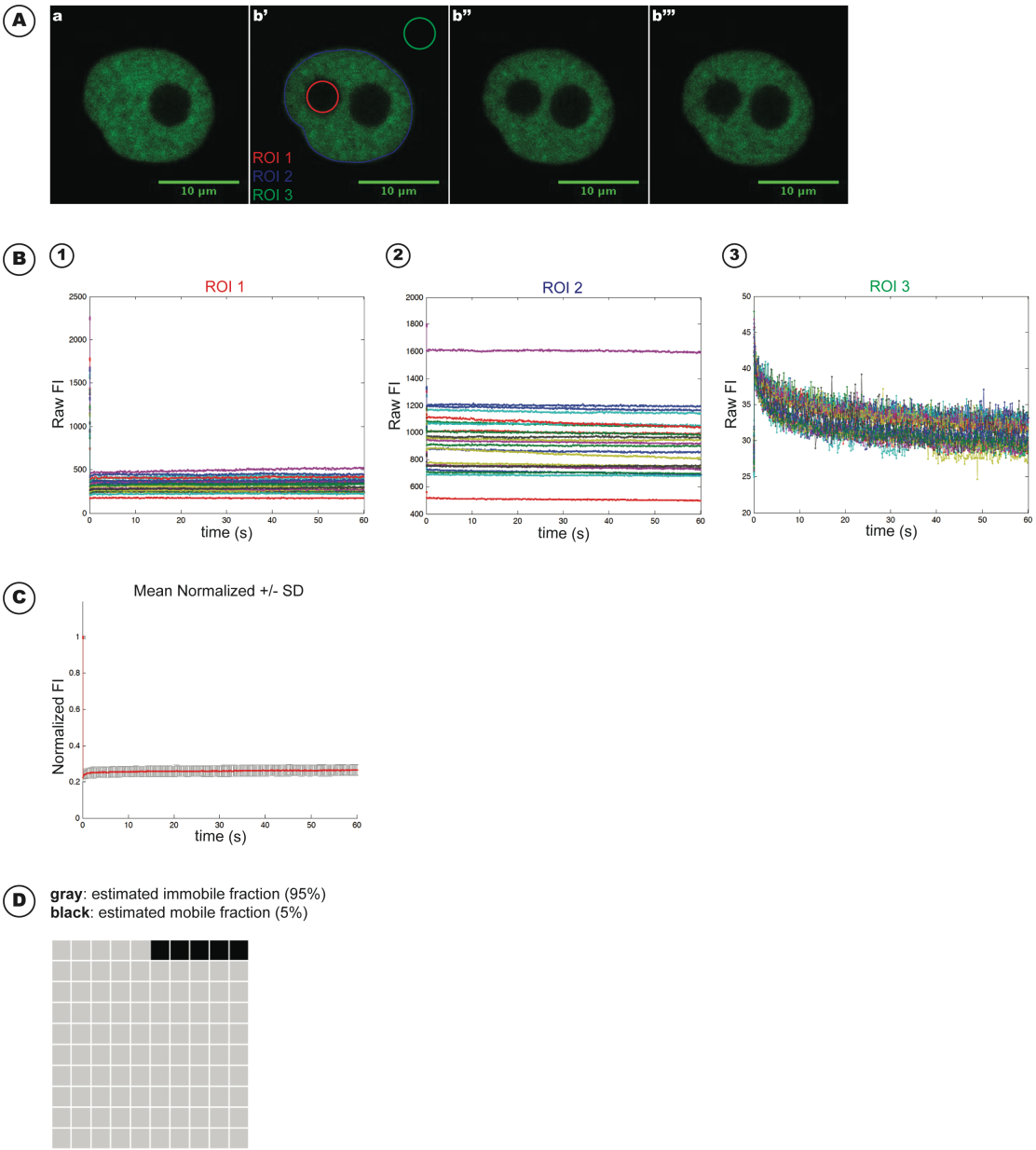

***Figure 3.3:* FRAP analysis for H3.2-eGFP in A6 cells**

*(**A**) Selected frames (scale bar: 10 µm) (**a**) prebleach (**b'**) postbleach 1 (0.154 s) (**b''**) postbleach 2 (30 s) (**b'''**) postbleach 3 (60 s)*

*(**B**) Fluorescence Intensity (FI) in (**1**) ROI1 (**2**) ROI2 (**3**) ROI3 for individual cell measurements (arbitrary units) • Bleaching Depth: 80% • Gap Ratio: 88%*

*(**C**) Mean normalized curves +/- SD • t/2: not calculable* • R^2: 98%*

*(**D**) Mobility Fractions (waffle chart)*

n = 23 cells from 2 independent experiments

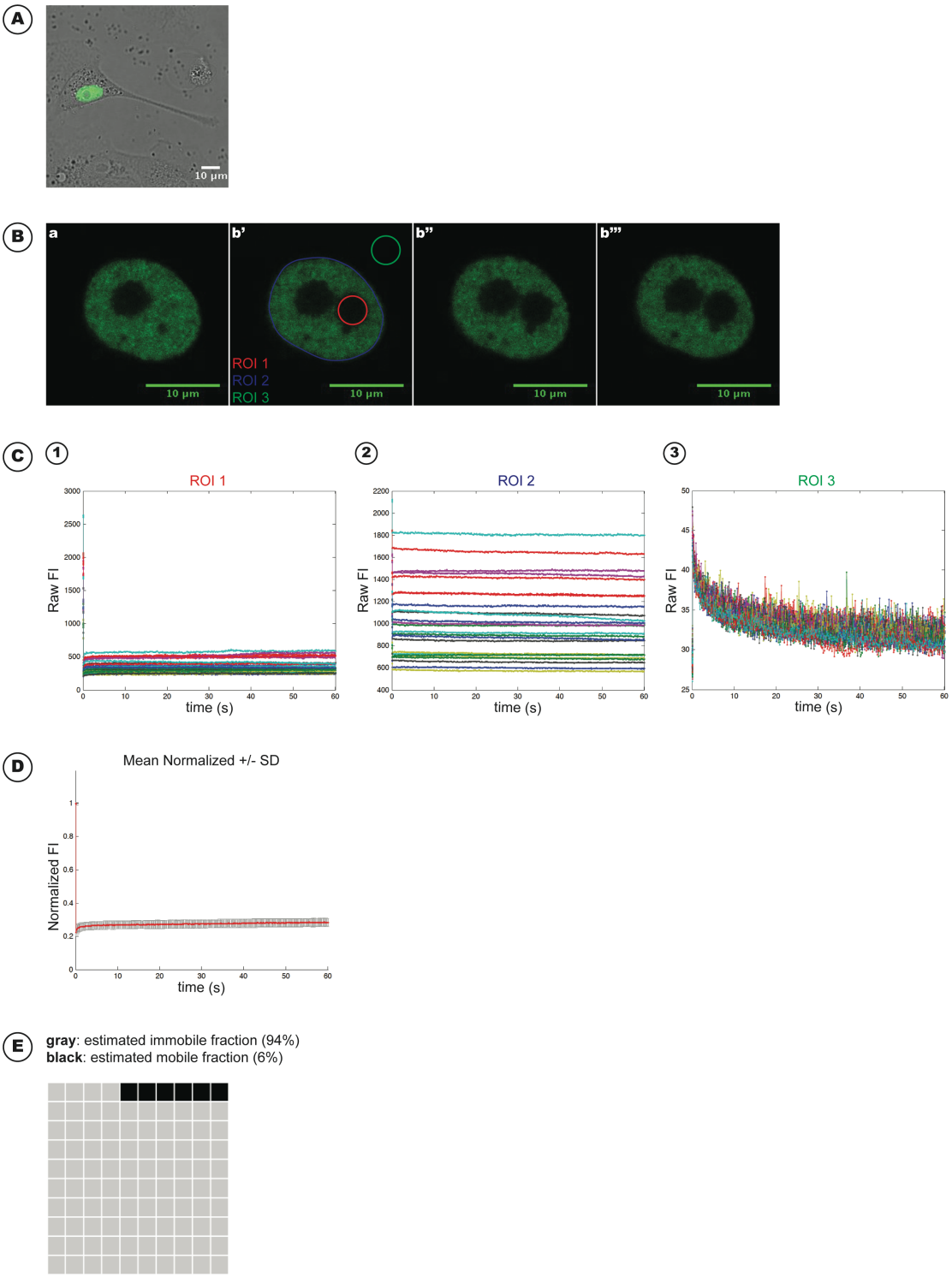

***Figure 3.4:* FRAP analysis for H3.3-eGFP in A6 cells**

*(**A**) Cell and nuclear morphology (brightfield + GFP, scale bar: 10 µm)*

*(**B**) Selected frames (scale bar: 10 µm) (**a**) prebleach (**b'**) postbleach 1 (0.154 s) (**b''**) postbleach 2 (30 s) (**b'''**) postbleach 3 (60 s)*

*(**C**) Fluorescence Intensity (FI) in (**1**) ROI1 (**2**) ROI2 (**3**) ROI3 for individual cell measurements (arbitrary units) • Bleaching Depth: 81% • Gap Ratio: 88%*

*(**D**) Mean normalized curves +/- SD • t/2: not calculable* • R^2: 97%*

*(**E**) Mobility Fractions (waffle chart)*
n = 25 cells from 2 independent experiments

We see almost no fluorescence recovery for H3.2-eGFP and H3.3-eGFP within the first 60 s after bleaching, the immobile fractions are 95% and 94%, respectively. Thus, we do not find any significant dynamic behavior for the two core histone variants H3.2 and H3.3 in somatic A6 cells. This behavior equates to that of these core histone variants in mammalian somatic HeLaK cells.

3.3) Applicability of embryos

When we started this project, our initial goal was to use embryos for FRAP analysis. To this end, embryos at different stages of development could be embedded in low melting agarose on a microscope slide and surface-proximal regions could be subjected to FRAP microscopy. We tested this method for the animal pole region of an embryo at late blastula (➤ *Figure 3.5*).

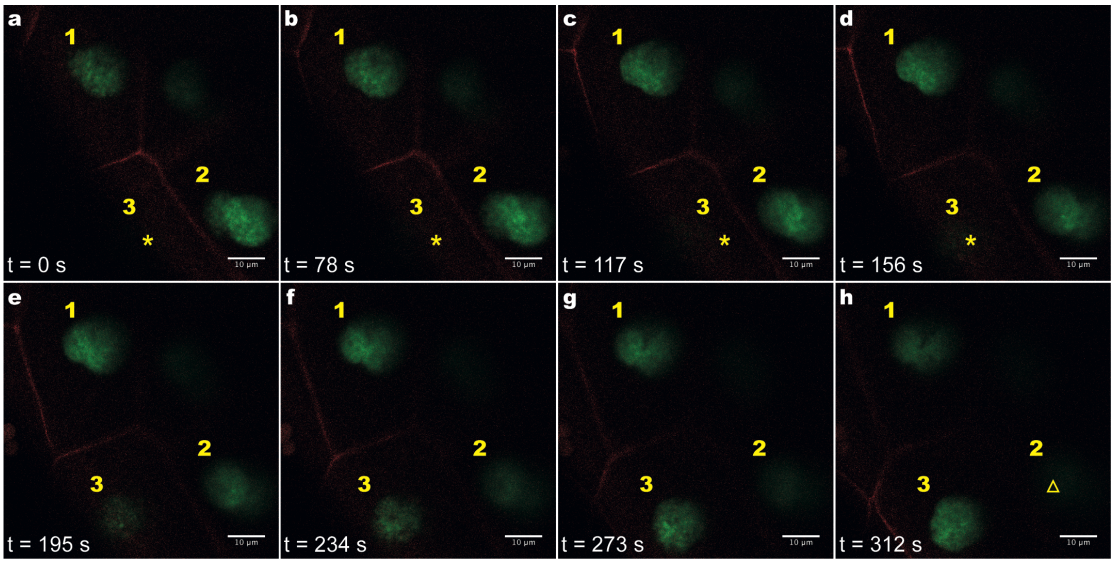

***Figure 3.5:* Animal pole region of a late blastula embryo (NF9)**
(time lapse over 5:12 min, scale bar: 10 µm)
The cell membrane (memRFP, faint) can be followed-up continuously, whereas none of the nuclei (H3.2-eGFP) keeps its position, although to differing extents: Nucleus 1 is trackable during the whole time lapse, yet slightly moves as the captured chromatin structure changes, nucleus 2 disappears (Δ), nucleus 3 emerges (*).

Analogous to Aoki et al., we see cell nuclei in motion, most likely due to cytoplasmic streaming. As a consequence, the registration of the image stack fails. Thus, these nuclei are inappropriate for FRAP experiments. This is line with the fact that cell membrane-associated

proteins have repeatedly been analyzed by FRAP (Eroshkin et al., 2016; Higashi et al., 2016) – in sharp contrast to nuclear or chromatin proteins in native embryonic cells.

In principle, three methodological approaches are conceivable to enable FRAP in *Xenopus*:

1. Cell nuclei are isolated from embryos or small embryonal dissections and attached to a microscopy slide by centrifugation. This method is already established (Aoki et al., 2010; Edens et al., 2017) but has conceptual shortcomings, as has been pointed out in *Chapter 1.4*.
2. Embryos are used and efforts are made to reduce nuclear motion by inhibition of the molecular mechanisms underlying cytoplasmic streaming.
3. Cells are isolated from embryos or small embryonal dissections and nuclear motion is possibly reduced by adherence on a microscopy slide, coated with a matrix yet to be found. It is conceivable that adherence leads to a change in the cell configuration in such a way that the range of motion of the cell nucleus within the cell is restricted and thus nuclear motion is reduced.

3.4) Novel method: Use of adherent animal cap cells

We considered it most promising to pursue the third option employing embryonic cells which have been isolated from animal caps. This implied that we had to find a substrate on which isolated animal cap cells adhere.

We discovered that animal cap cells adhere to a poly-L-lysine coated surface within the dissociation time (see experimental workflow). Whether cell adherence leads as well to a sufficient reduction of nuclear motion can be assessed only in the context of the first FRAP measurements.

Animal caps can be dissociated and animal cap cells can be isolated, respectively, by the removal of calcium. This is a commonly applied and *Xenopus*-specific method. Since we use cells of the non-pigmented inner cell layer, the animal cap has to be kept in a calcium-free, dissociating medium for another reason: The animal cap contracts from the beginning of dissection on, with the pigmented outer cell layer enclosing the inner cell layers. The experimental workflow is depicted and described in detail in the next figure.

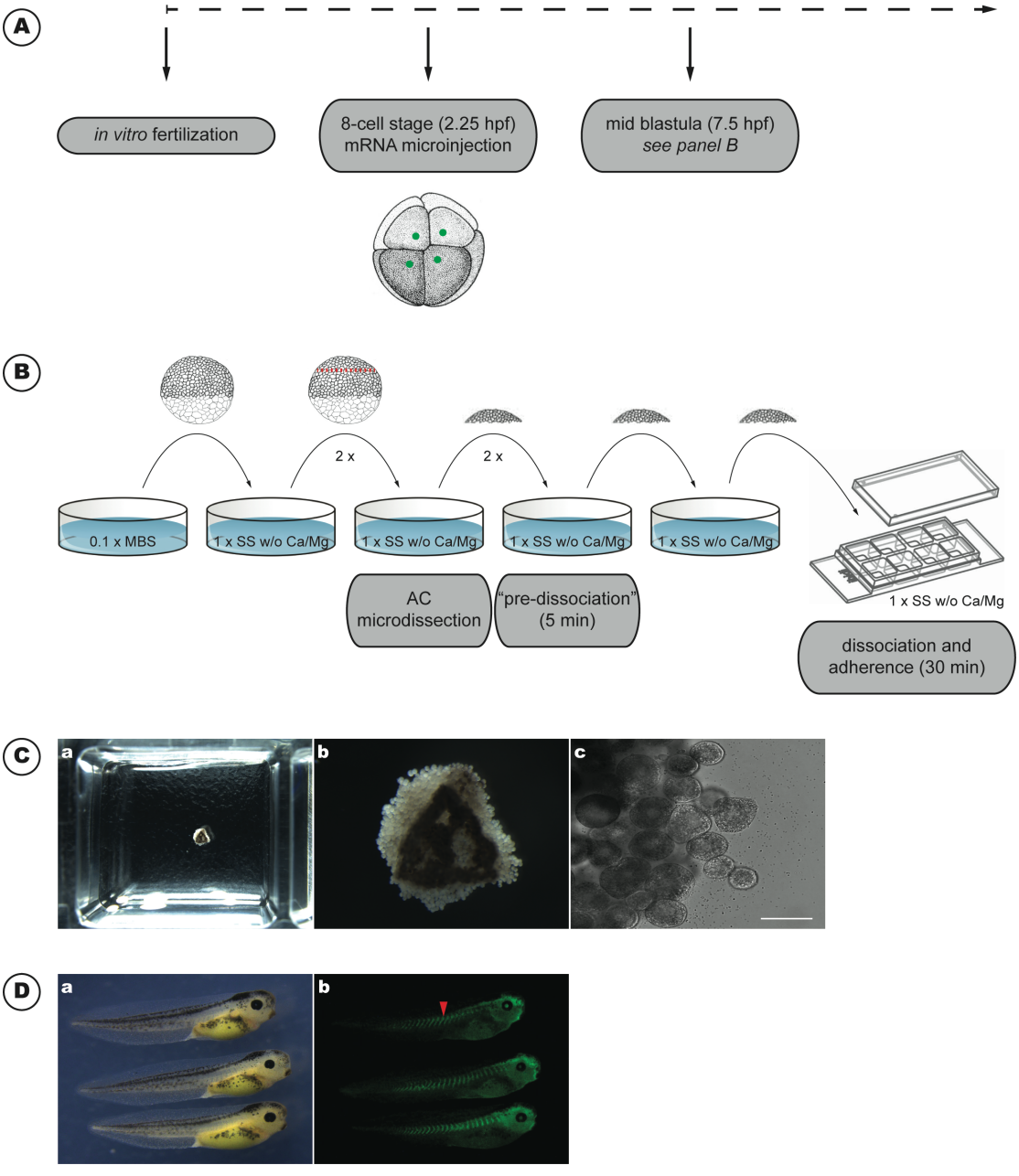

***Figure 3.6:* Experimental workflow**

*(**A**) **Part I:** mRNA is injected radially into the four animal blastomeres of an 8-cell embryo (2.25 hpf). We injected 500 pg mRNA/embryo, i.e. 125 pg mRNA/blastomere. Animal cap dissection starts at mid blastula (7.5 hpf).*

*(**B**) **Part II:** One embryo is selected and transferred to calcium- and magnesium-free, EDTA-supplemented 1 x Steinberg's solution. The embryos or animal caps are continuously kept in this medium from here on. The embryo is transferred two more times to reduce the calcium and magnesium ions transferred from the MBS solution. Residual calcium and magnesium ions are complexed by EDTA. The dissected animal cap is transferred three times to remove cell debris at the border zone of the animal cap. The cap then rests for approx. 5 minutes before being transferred into a well of a µ-slide®. A slightly "pre-dissociated", flatter animal*

cap is easier to transfer. The transfer of the animal cap into a well proceeds as follows: The animal cap is sucked approx. 5 mm into a glass capillary, which is then vertically immersed into the medium-filled well. The cap then descends slowly by gravity and usually orients itself "inner cell layer down". If the cap does not orient itself correctly, it is sucked up again and turned. This procedure is repeated for three more embryos. As a result, each of the four central wells of the 8 well µ-slide® is mounted with an animal cap. Dissection and mounting of four animal caps takes about 30 minutes. The mounted slide rests at room temperature for 30 minutes before the FRAP measurements can begin. These 30 minutes can be used to mount another slide. The animal cap cells burst on contact with air which must therefore be avoided (Potential caveat: air bubbles in the capillary).

*(**C**) Single well of a µ-slide® with a mounted animal cap at (**a**) low (**b**) high magnification (**c**) border zone of an animal cap (brightfield, scale bar: 50 µm)*

*(**D**) Injected embryos develop normally and show a regular phenotype (NF38). The usual mRNA-injection scheme has been applied (see above). The striking appearance of the somites (►) is due to the regular alignment of the nuclei in the center of the myocytes. (**a**) brightfield (**b**) H3.3-eGFP*

3.5) Ratio of soluble and chromatin-bound core histone molecules in blastula embryos

For somatic cells, we know that the vast majority of molecules of an individual core histone is incorporated into chromatin and thus is not soluble (about 99%) (Loyola et al., 2006). As we intend to investigate core histone dynamics in embryonic cells by a novel method yet to be established, it is helpful to first resort to an established molecular biological method and to differentiate the soluble and the non-soluble fraction of the entirety of molecules of individual core histones in embryonic cells. This experiment is also important for another reason: Since an additional, eGFP-tagged variant of the H3-variants is expressed, a situation of histone overload may be generated. Excess histones would be recorded as mobile and thus we would attain a false high mobility. To rule out histone overload, we have to show that the production of histone proteins from microinjected mRNA does not artefactually increase the non-incorporated pool. The experimental proceeding and the results are presented in the next figure.

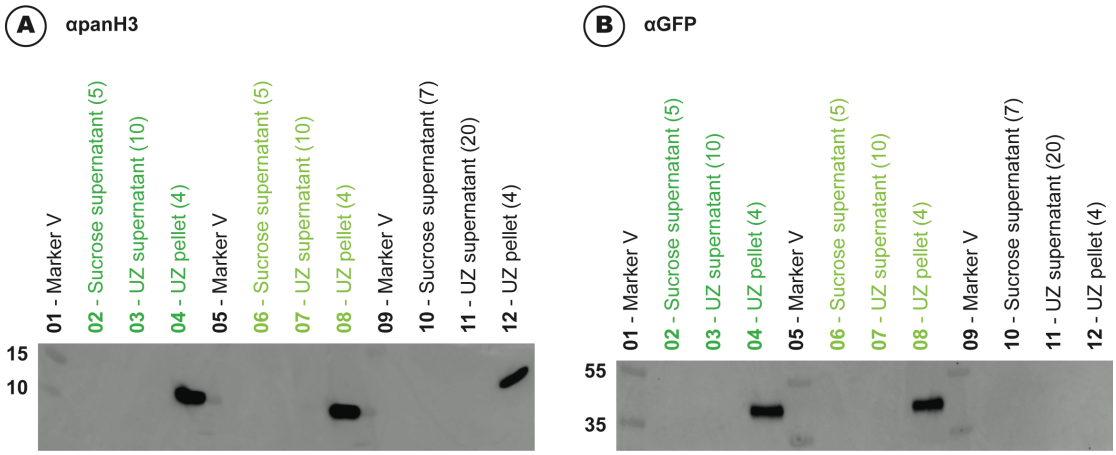

***Figure 3.7:* Western-blot**

dark green: H3.2-eGFP, light green: H3.3-eGFP, black: uninjected

(x): number of embryo equivalents loaded on gel

n = 3-5 independent experiments in each case

*(**A**) The same mRNA-injection scheme as for the following FRAP experiments has been applied (➤ Figure 3.6 A). We purified chromatin from isolated nuclei of blastula embryos according to the protocols detailed in Chapter 2.4.3. We then used a panH3-antibody to detect H3.2(-eGFP) and H3.3(-eGFP) in pure chromatin (UZ pellet), the nucleoplasm (UZ supernatant) and the cytoplasm (sucrose supernatant). Here we realized that the panH3 antibody does not detect eGFP-tagged H3, possibly for structural reasons. Therefore, we had to use a separate GFP-antibody (➤ B). As a result, H3.2 and H3.3 (both ~15 kDa) are detected exclusively in the pure chromatin fraction in both uninjected and injected embryos.*

*(**B**) We now applied a GFP-antibody to detect H3.2-eGFP and H3.3-eGFP in the three fractions. We see that H3.2-eGFP and H3.3-eGFP (both ~42 kDa) are detected again only in the pure chromatin fraction.*

Two important conclusions can be drawn from this experiment: First, virtually all molecules of H3.2 and H3.3 are chromatin-bound – as well in pluripotent embryonic cells. And second, even when up to 2.5-fold more material of supernatant than chromatin pellet was loaded on the gel, no histone proteins could be detected in the nucleoplasmic and cytoplasmic fractions of the injected embryos. Therefore, we do not generate histone overload from the dose of mRNA we inject.

Line profile plot

We additionally created a line profile plot, a Fiji application for the assessment of colocalization of two or more fluorescent proteins. This application extracts and plots relative values for the fluorescence intensity of the individual proteins along a defined line within a region of interest. Concordant curves are principally compatible with protein colocalization.

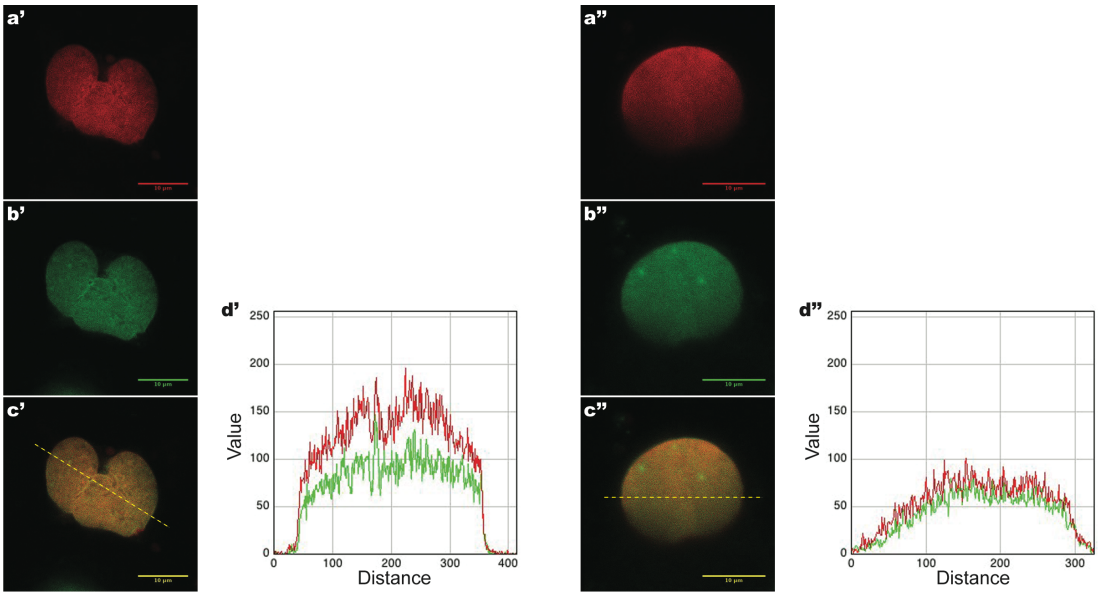

***Figure 3.8:* Line profile plot**

*Nuclei of adherent animal cap cells, expressing H3.2-eGFP or H3.3-eGFP. The same mRNA-injection scheme as for FRAP experiments has been applied (➤ Figure 3.6 A). DNA is stained with Hoechst 33342. The red curve represents the fluorescence intensity of Hoechst 33342 (DNA), the green curve the fluorescence intensity of the eGFP-tagged histones. (**a'+a"**) Hoechst 33342 (**b'**) H3.2-eGFP (**b"**) H3.3-eGFP (**c'+c"**) overlay (**d'+d"**) line profile plots (scale bar: 10 µm)*

Since we see largely concordant curves (*Figure 3.8*), a high degree of colocalization can be assumed which, with reservations, speaks as well for a high level of histone incorporation. However, it should be considered that only eGFP-tagged histones are captured, endogenous histones are not included. Further statements on histone incorporation and possible histone overload are therefore not possible.
The informative value of the Western-blot above is clearly higher. The line profile plot is introduced here nonetheless to provide a conceptual outline of this frequently used image analysis tool.

3.6) FRAP analyses for H3.2 and H3.3 in animal cap cells

We then applied our established protocol and were particularly interested in whether cell adherence also leads to a sufficient reduction of nuclear motion. The measurement settings used for the A6 cells have been adopted, except for the post bleaching time which has been halved in order to reduce the total laser exposure time. This parameter is relevant here insofar as the embryonic cells are relatively close to each other and possible scattering effects on neighboring cells have to therefore be considered. With these not substantially

altered settings we then conducted FRAP analyses for H3.2-eGFP and H3.3-eGFP (*Figure 3.9* and *Figure 3.10*).

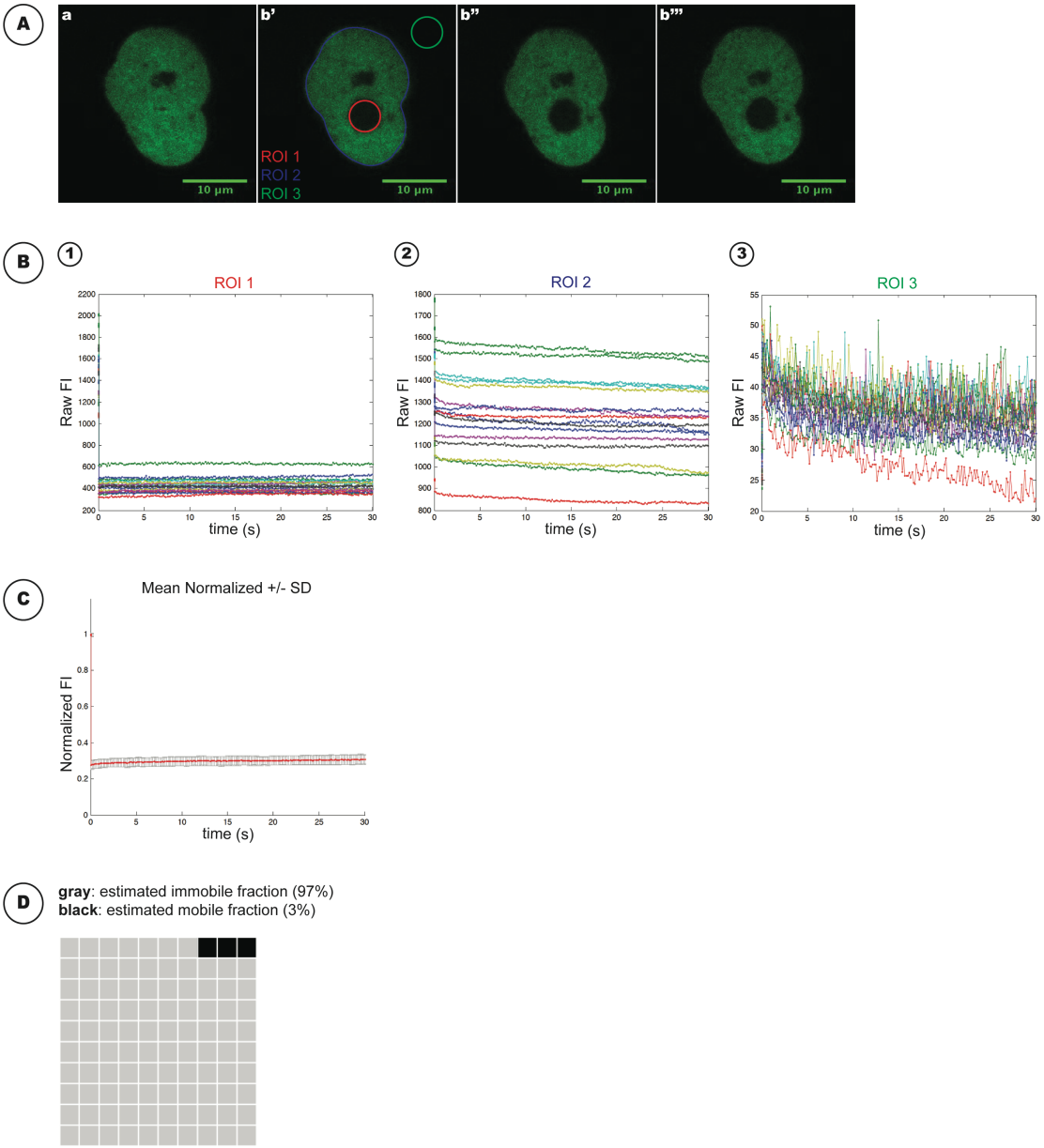

***Figure 3.9:* FRAP analysis for H3.2-eGFP in animal cap cells**

*(**A**) Selected frames (scale bar: 10 µm) (**a**) prebleach (**b'**) postbleach 1 (0.154 s) (**b''**) postbleach 2 (15 s) (**b'''**) postbleach 3 (30 s)*

*(**B**) Fluorescence Intensity (FI) in (**1**) ROI1 (**2**) ROI2 (**3**) ROI3 for individual cell measurements (arbitrary units) • Bleaching Depth: 75% • Gap Ratio: 91%*

*(**C**) Mean normalized curves +/- SD • t/2: not calculable* • R^2: 94%*

*(**D**) Mobility Fractions (waffle chart)*

n = 16 cells from 4 independent experiments

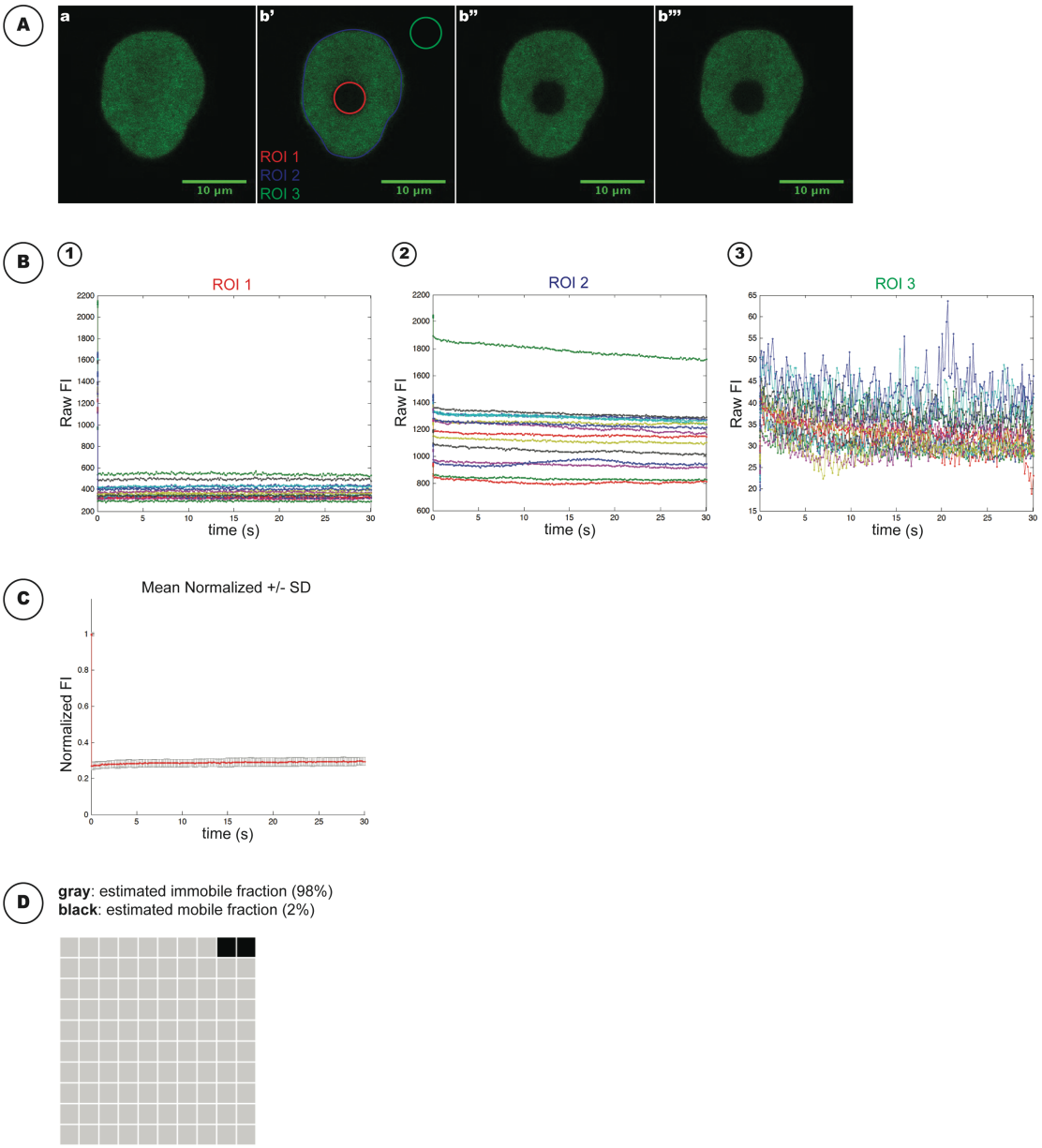

Figure 3.10: ***FRAP analysis for H3.3-eGFP in animal cap cells***

*(**A**) Selected frames (scale bar: 10 µm) (**a**) prebleach (**b'**) postbleach 1 (0.154 s) (**b''**) postbleach 2 (15 s) (**b'''**) postbleach 3 (30 s)*

*(**B**) Fluorescence Intensity (FI) in (**1**) ROI1 (**2**) ROI2 (**3**) ROI3 for individual cell measurements (arbitrary units) • Bleaching Depth: 76% • Gap Ratio: 91%*

*(**C**) Mean normalized curves +/- SD • t/2: not calculable* • R^2: 94%*

*(**D**) Mobility Fractions (waffle chart)*

n = 15 cells from 3 independent experiments

First, a brief glimpse at the nuclear architecture and chromatin structure is worthwhile: We see a *lobed* nucleus and a *fine-granular* chromatin (A). Both aspects differ from those of somatic cells and raise some questions to be discussed in *Chapter 4.3*: Are this nuclear

architecture and chromatin structure specific for pluripotent embryonic cells? How is the nuclear architecture structurally defined in these cells?

But our main focus is on the nuclear motion: The R-macro can easily register the cell nucleus in each individual frame. This means that the nuclear motion is sufficiently reduced by our novel methodological approach. This gives us a novel, working method. How the adherence leads to a reduction of the nuclear motion and whether the adherence is possibly accompanied by a change in the cell configuration, remains to be addressed separately.
The values achieved for the bleaching depth are around 80%, those for the gap ratio around 90%. Both values are within the reference range, which could not be predicted *a priori*, as the embryonic cells have a seminally different architecture compared to A6 cells. The satisfactory bleaching depth value can primarily be explained by the fact that cell nuclei were selected which are particularly close to the surface of the slide. It is also these nuclei which exhibit the highest degree of immobility.

If we now look at the results of the FRAP analyses, we see almost no fluorescence recovery for H3.2-eGFP and H3.3-eGFP within the first 30 s after bleaching, the immobile fractions are 97% and 98%, respectively. Thus, we do not register any significant dynamic behavior for the two core histone variants H3.2 and H3.3 in pluripotent embryonic cells. This behavior equates to that of these core histone variants in somatic A6 cells.

We interpret our results primarily independently of the measurement and culture temperature, respectively, which is 37°C for the HeLaK cells, 26°C for the A6 cells and 23°C for the embryonic cells, and thus covers a range of 14°C. Sophisticated diffusion models usually include temperature. However, the characterization of the dynamic behavior of individual chromatin components by FRAP analysis does not primarily require such a complex model. The determination of the two basic parameters t-half and mobility fractions is sufficient and is practiced here and in comparable studies (Meshorer et al., 2006; Boskovic et al., 2014). The calculation of these two parameters does not include the measurement temperature.

4) Discussion

If we recall the two objectives of this work formulated in *Chapter 1.5*, we recognize that both have been achieved: First, we have implemented the FRAP technique on pluripotent embryonic *Xenopus* cells. We use native, i.e. intact embryonic *Xenopus* cells – this is the key improvement over all previous approaches, for which Aoki et al. (2010) is representative (➤ *Chapter 1.4*). Secondly, we have used this novel method to characterize the two non-centromeric core histone H3 variants in *Xenopus*, H3.2 and H3.3, in pluripotent embryonic cells.

We have analyzed two core histone variants by FRAP, however, any other chromatin and nuclear component can be principally subjected to this technique and this method. The versatility of this system will allow to extent these observations throughout large parts of embryonic development (➤ *Chapter 4.4*), which promises interesting insights into the process of *chromatin maturation*. Some of the foundations of this process have already been deciphered using the model organism *Xenopus* (Akkers et al., 2009; Schneider et al., 2011; reviewed in Perino and Veenstra, 2016).

4.1) Core histone mobility in somatic cells

The soluble fraction of the entirety of molecules of an individual core histone variant in somatic mammalian HeLa S3 cells is approx. 1% (soluble nuclear: 0,6%, soluble cytosolic: 0,4%, chromatin-bound: 99%) (Loyola et al., 2006). This slight proportion is reflected in small mobile fractions of around 5% for core histones, which were obtained from FRAP analyses repeatedly in somatic mammalian cells (exemplarily Wiedemann et al., 2010) and in the present work in somatic amphibian cells.

Core histone provision in somatic cells has been recognized to be linear, “just in time” and precisely adapted to scheduled changes in demand. For replication-dependent core histone variants, this means that these histones are produced in near stochiometric abundance to the needs of the next S-phase (Gunjan et al., 2005; Marzluff et al., 2008). In addition, data from yeast provide evidence for the existence of regulated histone proteolysis (Gunjan et al., 2006). Thus, a pool of soluble core histones is basically not intended. Only histones in transit are transiently soluble, for example on the way from the ribosome to the nucleosome, as well as histones which are evicted during transcription or DNA repair.

However, this linearity between histone supply and demand can be perturbed: In the moment of a sudden and unanticipated increase of the mitosis rate and thus acute replication stress, the number of demanded histones transiently exceeds the amount of supplied histones. In the

case of mitosis inhibition, the reverse is true. Insufficient histone levels can trigger cell cycle arrest (Han et al., 1987; Kim et al., 1988; Nelson et al., 2002), whereas histone overload is linked to DNA damage and genome instability (Gunjan and Verreault, 2003).

Not surprisingly, the somatic cell has strategies to cushion, at least partially, imbalances in histone supply or demand. Cook et al. (2011) deciphered one of these strategies: NASP (nuclear autoantigenic sperm protein), a histone chaperone upstream to ASF1 (anti silencing factor 1) and CAF-1, balances a reservoir of NASP-associated but soluble H3-H4-heterodimers. NASP preserves H3-H4-dimers from being degraded. In case of histone shortage, the affinity of NASP towards H3-H4 is higher, so more H3-H4-dimers are preserved from degradation. In case of histone overload or perturbation of ASF1 activity, the affinity of NASP towards H3-H4 is lower and thus H3-H4-dimers are more likely to be degraded.

4.2) Core histone mobility in totipotent and pluripotent embryonic cells

We were able to show by Western-blot analysis that the "Loyola paradigm" (➤ *Chapter 4.1*) also applies to pluripotent embryonic *Xenopus* cells: The core histone variants H3.2 and H3.3 are almost exclusively chromatin-bound. In addition, we were able to show by FRAP analysis that the non-soluble fraction of these two histones is more than 95% each.

If we now look at which mobilities for H3 variants were measured in comparable studies in other model systems, the picture is not quite uniform: Meshorer et al. (2006) see no significant mobility for H3.3, but a moderately elevated mobile fraction of approx. 25% for canonical H3 in pluripotent ES cells. Boskovic, Torres-Padilla et al. (2014), which use totipotent embryonic mouse cells (see below), see a moderately increased mobile fraction of approx. 25% for the two canonical variants H3.1 and H3.2 in 2-cell embryos, which has fallen to approx. 5% already in 8-cell embryos. For H3.3, a mobile fraction of approx. 5% is seen throughout. The existing discrepancy regarding the mobility of canonical H3 cannot be resolved for now, however our analyses support the Boskovic results.

The group around M.-E. Torres-Padilla were pioneers in using totipotent mouse pre-implantation embryos for FRAP microscopy. The study just mentioned above is one of the studies using this novel method. Therein the three non-centromeric mammalian H3 variants H3.1, H3.2 and H3.3 are characterized in 2-cell and 8-cell embryos. H3.3, whose role is seen rather in the context of transcriptional gene activation, is the predominant H3 variant in the mouse zygote (Torres-Padilla et al., 2006; Santenard et al., 2010; Akiyama et al., 2011). Within the first three cell divisions, H3.3 is replaced “in a global wave of incorporation” (Boskovic et al., 2014) by the replication-dependent, canonical variants H3.1 and H3.2, which

are assigned a more repressive role. In this context, H3.3 is also referred to as a “placeholder” (Akiyama et al., 2011; Dunleavy et al., 2011).

We do not yet know whether the situation in *Xenopus* is comparable to that in the mouse, i.e. whether H3.3 is the predominant H3 variant as well in totipotent *Xenopus* embryos and whether a global replacement by H3.2 follows. Besides, it is questionable whether FRAP measurements on totipotent embryonic *Xenopus* cells are feasible at all, as these have a different size and morphology compared to pluripotent embryonic cells. Nonetheless, from the synopsis of our results and those of Boskovic et al. we can draw two conclusions regarding chromatin dynamics in general and core histone dynamics in particular:

1. The starting point is a developmental biological motif which here could be defined as follows: Cell differentiation is driven by a gradual repression of the genome by epigenetic mechanisms (Müller and Leutz, 2001; Eckfeldt et al., 2005). Besides an increasing DNA methylation and a gradual increase of repressive posttranslational histone modifications, for example, the replacement of “activating” by “repressive” histone variants plays a fundamental role here. This is exemplified by the global replacement of H3.3 by canonical H3 variants in totipotent 2-cell and 4-cell mouse embryos.
   In the setting of a histone variant replacement, at least two variants compete for one chromatin binding site, i.e. at least one variant is always (transiently) soluble in the sense of being non-incorporated and thus can be detected and quantified by FRAP.

2. In totipotent embryonic mouse cells, the replacement of the initially predominant H3.3 by the two canonical H3 variants within the first three cell divisions is described as “wave-like” (see above). The FRAP analyses by Boskovic et al. reveal a moderately increased soluble fraction of approx. 25% for the, one might say *hyperdynamic*, canonical variants in totipotent embryonic cells.
   In the context of mapping of posttranslational histone modifications during *Xenopus* development by mass spectrometry, Schneider et al. (2011) also determined the H3.2-to-H3.3 ratio. From this work we know that H3.2 is the predominant H3 variant in pluripotent late blastula *Xenopus* embryos (H3.2/H3.3 ratio: 80/20%), the earliest stage examined here. H3.3 is then gradually and almost completely replaced over a long developmental period, a process which does not end before tadpole stage. Our FRAP analyses do *not* indicate an enhanced mobility for the canonical variant H3.2 in pluripotent embryonic cells.

Thus, a global replacement of a core histone variant within few cell cycles is one of probably a number of cellular processes still to be identified which can be assumed to be fundamental for a (hyper)dynamic behavior of individual core histone variants in early embryonic cells.

4.3) Nuclear architecture and chromatin structure in pluripotent embryonic cells

Nuclear architecture

The *lobed* architecture of the nucleus in pluripotent embryonic *Xenopus* cells is reflected in the description of an “ill-defined” nuclear lamina in pluripotent ES cells which acquires a “round and distinct” character in lineage-committed NP cells (Meshorer and Misteli, 2006). Thus, this aspect of the nucleus seems to be specific for pluripotent embryonic cells.

Metazoan cell nuclei are delimited by the *nuclear envelope* (NE) which is built up from two lipid membranes with integrated pore complexes, and a *nuclear lamina* that lies close to the inner lipid membrane. The nuclear lamina is a meshwork of type V intermediate filaments, the so-called nuclear *lamins*. Vertebrates express two types of lamins, lamin A and lamin B. Lamin A has been shown to be absent in mouse and human pluripotent ES cells. Moreover, lamin A is seen to be “indicative” for pluripotency (Constantinescu et al., 2006). Both lamin proteins directly associate with chromatin which is stabilized by the nuclear lamina (Taniura et al., 1995; Melcer et al., 2012; Mattout et al., 2007).

Specific mutations in the gene for lamin A (LMNA) are associated with a group of rare, hereditary diseases, the laminopathies. These so-called “orphan-diseases” increasingly manifest after birth and often lead to premature death. This group includes, to name just a few examples, muscular dystrophy, cardiomyopathy, dyslipidemia and progeria, all to varying degrees and in varying combinations (Mattout et al., 2006; Hutchison and Worman, 2004; Gruenbaum et al., 2005; Rankin and Ellard, 2006).

Schäpe et al. (2009) examined the contribution of prelamin A to the rigidity or “stiffness” of the nucleus. Therein, lamin A was ectopically expressed in *X. laevis* oocytes and the rigidity of the nuclear envelope was analyzed by atomic force microscopy. This experiment revealed that a high expression of prelamin A is concomitant with a more rigid nuclear envelope. Assuming that the *lobed* aspect of the cell nucleus is founded in structural-morphological causes, then this unique architecture might be explained by the absence of lamin A.

Beyond that, we increasingly understand the mechanisms which control nuclear size in embryonic cells, not least in the light of two recent *Xenopus* studies: Brownlee and Heald (2019) postulate that nuclear size reduction before mid-blastula transition (MBT) is driven, at least partially, through palmitoylation of the nuclear transport factor importin α, subsequent sequestration of palmitoylated importin α into the plasma membrane, and thus, reduced levels of cytoplasmic importin α and reduced nuclear import kinetics. Nuclear size reduction from MBT on has also been connected to phosphorylation of a single serine residue of lamin B3 (S267) by conventional protein kinase C (cPKC) (Edens et al., 2017).

Chromatin structure

With regard to the *fine-granular* chromatin structure in pluripotent embryonic *Xenopus* cells, this is in line with the observation of a “more diffuse” chromatin structure in pluripotent ES cells which changes to a “more compact” structure with “well defined foci” in lineage-committed NP cells (Meshorer and Misteli, 2006). The intensity of heterochromatic histone modifications as well as the number of heterochromatic foci increases, whereas the size of heterochromatic foci decreases (Meshorer et al., 2006). This view is supported by the reduced levels of heterochromatic histone modifications found in pluripotent *Xenopus* blastula cells (Akkers et al., 2009; Schneider et al., 2011). Thus, in addition to the *lobed* aspect of the cell nucleus, the *fine-granular* chromatin structure appears to be another specific feature of pluripotent embryonic cells.

4.4) Future directions

4.4.1) Including further embryonic stages

It would be preferable to include embryonic cells beyond the blastula stage into FRAP analyses. However, it should be considered that the dissociation efficiency decreases as embryonic development progresses. Optimized dissociation conditions would therefore be desirable. With this aim Briggs et al. (2018) tested partly already used, partly newly composed dissociation media. The highest dissociation efficiency is attributed to the so-called "Newport 2.0" buffer.

“Newport 2.0” differs from the standard Newport buffer by the supplementation of the buffer reagent 3-(Cyclohexylamino)-1-propanesulfonic acid (CAPS) and raising of the pH from 9.0 to 10.5. This allows complete dissociation of embryos from NF8 (blastula) up to and including NF22 (early tailbud) in less than half an hour. The authors suggest a possibly increased dissociation constant of the calcium ions as well as a possible non-specific surface protein denaturation as causal for this increased dissociation efficiency.

With these improved dissociation conditions, it should be possible to create a close-meshed temporal map of histone protein mobility from pluripotent to differentiated somatic states.

4.4.2) Using embryos

As pointed out in *Chapter 3.3*, to our understanding, embryos can only be used for FRAP microscopy, if a reduction of nuclear motion is achieved by inhibition of the molecular mechanisms underlying cytoplasmic streaming. As described in *Chapter 1.4*, it is the motor proteins moving on the cytoskeleton which generate cytoplasmic streaming. An inhibition of

cytoplasmic streaming must therefore start at this point. The following study is informative in this context:

Foissner and Wasteneys (2000) investigated the effect of cytochalasin D in ascending concentrations (0.1-8 µM) (-/+ 10 µM oryzalin or 5 µM colchicine) on the disassembly and reassembly of actin filaments and microtubules as well as on the reduction of cytoplasmic streaming in internode cells of *Charophyceae* ("chandelier algae"). The mycotoxin cytochalasin D inhibits actin filament polymerization, the herbicide oryzalin and the "mitosis-inhibitor" colchicine disrupt microtubule formation. As a result, treatment with 8 µM cytochalasin D alone inhibits cytoplasmic streaming within a few minutes. In addition, the actin filaments reassemble within a short time after the removal of cytochalasin D. The cytoplasmic streaming is then restored. When cytochalasin D is combined with 10 µM oryzalin or 5 µM colchicine, a dose of 2.8 µM is sufficient to inhibit cytoplasmic streaming. In this case as well, cytoplasmic streaming is reestablished within a short time after the removal of the agents.

Three aspects are remarkable here: the short incubation time, the fast and complete reversibility as well as the possibility to combine several agents and thus to reduce the toxicity of each individual agent. Should these inhibitors stop cytoplasmic streaming as well in cells of the *Xenopus* embryo, one might be able to subject surface-proximal regions to FRAP analysis at essentially each instant during development.

Appendix I: Abbreviations

AOTF	acousto-optical tunable filter
ATP	adenosine triphosphate
au	arbitrary unit
AU	airy unit
bp	base pair
ddH_2O	double distilled H_2O
DEPC	diethylpyrocarbonate
DNA	deoxyribonucleic acid
dNTP	deoxynucleoside 5'-triphosphate
DTT	dithiothreitol
EDTA	ethylenediaminetetraacetic acid
epiSC	epiblast stem cell
ES cell	embryonic stem cell
for	forward
FRAP	fluorescence recovery after photobleaching
(e)GFP	(enhanced) green fluorescent protein
HeLaK	HeLa Kyoto
HEPES	2-(4-(2-Hydroxyethyl)-1-piperazinyl) ethanesulfonic acid
hpf	hours post fertilisationem
Hz	Hertz
kDa	kilo Dalton
MBT	mid-blastula transition
me	methylation
MeOH	methanol
NF	Nieuwkoop and Faber
NP cell	neural precursor cell
NP-40	nonylphenol 40
NTP	nucleoside 5'-triphosphate
PBS	phosphate-buffered saline
PCR	polymerase chain reaction
psi	pound-force per square inch
PTM	posttranslational modification
px	pixel
rev	reverse
(m)RNA	(messenger) ribonucleic acid
rpm	revolutions per minute
SD	standard deviation
SDS	sodium dodecyl sulfate

TBS	TRIS-buffered saline
TE buffer	TRIS-EDTA buffer
TRIS	tris(hydroxymethyl)-aminomethan (THAM)
V	Volt
w/o	without

Appendix II: References

Akiyama T, Suzuki O, Matsuda J, Aoki F (2011) Dynamic replacement of histone H3 variants reprograms epigenetic marks in early mouse embryos. *PLoS Genetics*, **7**, e1002279.

Akkers RC, van Heeringen SJ, Jacobi UG, Janssen-Megens EM, Françoijs KJ, Stunnenberg HG, Veenstra GJ (2009) A hierarchy of H3K4me3 and H3K27me3 acquisition in spatial gene regulation in Xenopus embryos. *Developmental Cell*, **17**, 425-34.

Aoki R, Inui M, Hayashi Y, Sedohara A, Okabayashi K, Ohnuma K, Murata M, Asashima M (2010) An in vitro reconstitution system for the assessment of chromatin protein fluidity during Xenopus development. *Biochemical and Biophysical Research Communications*, **400**, 200-6.

Axelrod D, Elson EL, Schlessinger J, Koppel DE (2018) Reminiscences on the "Classic" 1976 FRAP Article in Biophysical Journal. *Biophysical Journal*, **115**, 1156-9.

Axelrod D, Koppel DE, Schlessinger J, Elson E, Webb WW (1976) Mobility measurement by analysis of fluorescence photobleaching recovery kinetics. *Biophysical Journal*, **16**, 1055-69.

Behjati S, Tarpey PS, Presneau N, Scheipl S, Pillay N, Van Loo P, Wedge DC, Cooke SL, Gundem G, Davies H et al. (2013) Distinct H3F3A and H3F3B driver mutations define chondroblastoma and giant cell tumor of bone. *Nature Genetics*, **45**, 1479-82.

Bhaumik SR, Smith E, Shilatifard A (2007) Covalent modifications of histones during development and disease pathogenesis. *Nature Structural & Molecular Biology*, **14**, 1008-16.

Boskovic A, Eid A, Pontabry J, Ishiuchi T, Spiegelhalter C, Raghu Ram EV, Meshorer E, Torres-Padilla ME (2014) Higher chromatin mobility supports totipotency and precedes pluripotency in vivo. *Genes & Development*, **28**, 1042-7.

Briggs JA, Weinreb C, Wagner DE, Megason S, Peshkin L, Kirschner MW, Klein AM (2018) The dynamics of gene expression in vertebrate embryogenesis at single-cell resolution. *Science*, **360**.

Brownlee C, Heald R (2019) Importin α Partitioning to the Plasma Membrane Regulates Intracellular Scaling. *Cell*, **176**, 805-15.

Buschbeck M, Hake SB (2017) Variants of core histones and their roles in cell fate decisions, development and cancer. *Nature Reviews Molecular Cell Biology*, **18**, 299-314.

Chalfie M, Tu Y, Euskirchen G, Ward WW, Prasher DC (1994) Green fluorescent protein as a marker for gene expression. *Science*, **263**, 802-5.

Cheung P, Allis CD, Sassone-Corsi P (2000) Signaling to chromatin through histone modifications. *Cell*, **103**, 263-71.

Ciocanel MV, Kreiling JA, Gagnon JA, Mowry KL, Sandstede B (2017) Analysis of Active Transport by Fluorescence Recovery after Photobleaching. *Biophysical Journal*, **112**, 1714-25.

Cole NB, Smith CL, Sciaky N, Terasaki M, Edidin M, Lippincott-Schwartz J (1996) Diffusional mobility of Golgi proteins in membranes of living cells. *Science*, **273**, 797-801.

Constantinescu D, Gray HL, Sammak PJ, Schatten GP, Csoka AB (2006) Lamin A/C expression is a marker of mouse and human embryonic stem cell differentiation. *Stem Cells*, **24**, 177-85.

Cook AJ, Gurard-Levin ZA, Vassias I, Almouzni G (2011) A specific function for the histone chaperone NASP to fine-tune a reservoir of soluble H3-H4 in the histone supply chain. *Molecular Cell*, **44**, 918-27.

Cubitt AB, Heim R, Adams SR, Boyd AE, Gross LA, Tsien RY (1995) Understanding, improving and using green fluorescent proteins. *Trends in Biochemical Sciences*, **20**, 448-55.

Drané P, Ouararhni K, Depaux A, Shuaib M, Hamiche A (2010) The death-associated protein DAXX is a novel histone chaperone involved in the replication-independent deposition of H3.3. *Genes & Development*, **24**, 1253-65.

Dunleavy EM, Almouzni G, Karpen GH (2011) H3.3 is deposited at centromeres in S phase as a placeholder for newly assembled CENP-A in G_1 phase. *Nucleus*, **2**, 146-57.

Dyer MA, Qadeer ZA, Valle-Garcia D, Bernstein E (2017) ATRX and DAXX: Mechanisms and Mutations. *Cold Spring Harbor Perspectives in Medicine*, **7**.

Eckfeldt CE, Mendenhall EM, Verfaillie CM (2005) The molecular repertoire of the 'almighty' stem cell. *Nature Reviews Molecular Cell Biology*, **6**, 726-37.

Edens LJ, Dilsaver MR, Levy DL (2017) PKC-mediated phosphorylation of nuclear lamins at a single serine residue regulates interphase nuclear size in *Xenopus* and mammalian cells. *Molecular Biology of the Cell*, **28**, 1389-99.

Edginton AN, Rouleau C, Stephenson GR, Boermans HJ (2007) 2,4-D butoxyethyl ester kinetics in embryos of Xenopus laevis: the role of the embryonic jelly coat in reducing chemical absorption. *Archives of Environmental Contamination and Toxicology*, **52**, 113-20.

Efroni S, Duttagupta R, Cheng J, Dehghani H, Hoeppner DJ, Dash C, Bazett-Jones DP, Le Grice S, McKay RD, Buetow KH et al. (2008) Global transcription in pluripotent embryonic stem cells. *Cell Stem Cell*, **2**, 437-47.

Eroshkin FM, Nesterenko AM, Borodulin AV, Martynova NY, Ermakova GV, Gyoeva FK, Orlov EE, Belogurov AA, Lukyanov KA, Bayramov AV, Zaraisky AG (2016) Noggin4 is a long-range inhibitor of Wnt8 signalling that regulates head development in Xenopus laevis. *Scientific Reports*, **6**, 23049.

Fan Y, Nikitina T, Morin-Kensicki EM, Zhao J, Magnuson TR, Woodcock CL, Skoultchi AI (2003) H1 linker histones are essential for mouse development and affect nucleosome spacing in vivo. *Molecular and Cellular Biology*, **23**, 4559-72.

Fan Y, Nikitina T, Zhao J, Fleury TJ, Bhattacharyya R, Bouhassira EE, Stein A, Woodcock CL, Skoultchi AI (2005) Histone H1 depletion in mammals alters global chromatin structure but causes specific changes in gene regulation. *Cell*, **123**, 1199-212.

Foissner I, Wasteneys GO (2000) Microtubule disassembly enhances reversible cytochalasin-dependent disruption of actin bundles in characean internodes. *Protoplasma*, **214**, 33-44.

Goldberg AD, Banaszynski LA, Noh KM, Lewis PW, Elsaesser SJ, Stadler S, Dewell S, Law M, Guo X, Li X et al. (2010) Distinct factors control histone variant H3.3 localization at specific genomic regions. *Cell*, **140**, 678-91.

Goldstein RE, van de Meent JW (2015) A physical perspective on cytoplasmic streaming. *Interface Focus*, **5**, 20150030.

Greb C (2012) Basic Principles of Luminescence. *Leica online tutorial*.

Gunjan A and Verreault A (2003) A Rad53 kinase-dependent surveillance mechanism that regulates histone protein levels in S. cerevisiae. *Cell*, **115**, 537-49.

Gunjan A, Paik J, Verreault A (2005) Regulation of histone synthesis and nucleosome assembly. *Biochimie*, **87**, 625-35.

Gunjan A, Paik J, Verreault A (2006) The emergence of regulated histone proteolysis. *Current Opinion in Genetics & Development*, **16**, 112-8.

Gurdon JB, Melton DA (2008) Nuclear reprogramming in cells. *Science*, **322**, 1811-5.

Gruenbaum Y, Margalit A, Goldman RD, Shumaker DK, Wilson KL (2005) The nuclear lamina comes of age. *Nature Reviews Molecular Cell Biology*, **6**, 21-31.

Higashi T, Arnold TR, Stephenson RE, Dinshaw KM, Miller AL (2016) Maintenance of the Epithelial Barrier and Remodeling of Cell-Cell Junctions during Cytokinesis. *Current Biology*, **26**, 1829-42.

Hake SB, Allis CD (2006) Histone H3 variants and their potential role in indexing mammalian genomes: the "H3 barcode hypothesis". *PNAS*, **103**, 6428-35.

Han M, Chang M, Kim UJ, Grunstein M (1987) Histone H2B repression causes cell-cycle-specific arrest in yeast: effects on chromosomal segregation, replication, and transcription. *Cell*, **48**, 589-97.

Heim R, Cubitt AB, Tsien RY (1995) Improved green fluorescence. *Nature*, **373**, 663-4.

Hung T, Chang HY (2010) Long noncoding RNA in genome regulation: prospects and mechanisms. *RNA Biology*, **7**, 582-5.

Hutchison CJ, Worman HJ (2004) A-type lamins: guardians of the soma? *Nature Cell Biology*, **6**, 1062-7.

Jenuwein T, Allis CD (2001) Translating the histone code. *Science*, **293**, 1074-80.

Khuong-Quang DA, Buczkowicz P, Rakopoulos P, Liu XY, Fontebasso AM, Bouffet E, Bartels U, Albrecht S, Schwartzentruber J, Letourneau L et al. (2012) K27M mutation in histone H3.3 defines clinically and biologically distinct subgroups of pediatric diffuse intrinsic pontine gliomas. *Acta neuropathologica*, **124**, 439-47.

Kim UJ, Han M, Kayne P, Grunstein M (1988) Effects of histone H4 depletion on the cell cycle and transcription of Saccharomyces cerevisiae. *EMBO Journal*, **7**, 2211-9.

Kouzarides T (2007) Chromatin modifications and their function. *Cell*, **128**, 693-705.

Koziol MJ, Rinn JL (2010) RNA traffic control of chromatin complexes. *Current Opinion in Genetics & Development*, **20**, 142-8.

Lewis PW, Elsaesser SJ, Noh KM, Stadler SC, Allis CD (2010) Daxx is an H3.3-specific histone chaperone and cooperates with ATRX in replication-independent chromatin assembly at telomeres. *PNAS*, **107**, 14075-80.

Li X, Tyler JK (2016) Nucleosome disassembly during human non-homologous end joining followed by concerted HIRA- and CAF-1-dependent reassembly. *Elife*, **5**, e15129.

Lippincott-Schwartz J, Snapp EL, Phair RD (2018) The Development and Enhancement of FRAP as a Key Tool for Investigating Protein Dynamics. *Biophysical Journal*, **115**, 1146-55.

Loyola A, Bonaldi T, Roche D, Imhof A, Almouzni G (2006) PTMs on H3 variants before chromatin assembly potentiate their final epigenetic state. *Molecular Cell*, **24**, 309-16.

Luger K, Mäder AW, Richmond RK, Sargent DF, Richmond TJ (1997) Crystal structure of the nucleosome core particle at 2.8 A resolution. *Nature*, **389**, 251-60.

MacAlpine DM, Almouzni G (2013) Chromatin and DNA replication. *Cold Spring Harbor Perspectives in Biology*, **5**, a010207.

Marzluff WF, Wagner EJ, Duronio RJ (2008) Metabolism and regulation of canonical histone mRNAs: life without a poly(A) tail. *Nature Reviews Genetics*, **9**, 843-54.

Mattout A, Dechat T, Adam SA, Goldman RD, Gruenbaum Y (2006) Nuclear lamins, diseases and aging. *Current Opinion in Cell Biology*, **18**, 335-41.

Mattout A, Goldberg M, Tzur Y, Margalit A, Gruenbaum Y (2007) Specific and conserved sequences in D. melanogaster and C. elegans lamins and histone H2A mediate the attachment of lamins to chromosomes. *Journal of Cell Science*, **120**, 77-85.

Melcer S, Hezroni H, Rand E, Nissim-Rafinia M, Skoultchi A, Steward CL, Bustin M, Meshorer E (2012) Histone modifications and lamin A regulate chromatin protein dynamics in early embryonic stem cell differentiation. *Nature Communications*, **3**, 910.

Meshorer E, Misteli T (2006) Chromatin in pluripotent embryonic stem cells and differentiation. *Nature Reviews Molecular Cell Biology*, **7**, 540-6.

Meshorer E, Yellajoshula D, George E, Scambler PJ, Brown DT, Misteli T (2006) Hyperdynamic plasticity of chromatin proteins in pluripotent embryonic stem cells. *Developmental Cell*, **10**, 105-16.

Misteli T, Gunjan A, Hock R, Bustin M, Brown DT (2000) Dynamic binding of histone H1 to chromatin in living cells. *Nature*, **408**, 877-81.

Misteli T, Spector DL (1997) Applications of the green fluorescent protein in cell biology and biotechnology. *Nature Biotechnology*, **15**, 961-4.

Müller C, Leutz A (2001) Chromatin remodeling in development and differentiation. *Current Opinion in Genetics & Development*, **11**, 167-74.

Nacev BA, Feng L, Bagert JD, Lemiesz AE, Gao J, Soshnev AA, Kundra R, Schultz N, Muir TW, Allis CD (2019) The expanding landscape of 'oncohistone' mutations in human cancers. *Nature*, **567**, 473-8.

Nelson DM, Ye X, Hall C, Santos H, Ma T, Kao GD, Yen TJ, Harper JW, Adams PD (2002) Coupling of DNA synthesis and histone synthesis in S phase independent of cyclin/cdk2 activity. *Molecular and Cellular Biology*, **22**, 7459-72.

Okabayashi K, Asashima M (2006) In Vitro organogenesis using amphibian pluripotent cells. *Proceedings of the Japan Academy, Series B, Physical and Biological Sciences*, **82**, 197-207.

Perino M, Veenstra GJ (2016) Chromatin Control of Developmental Dynamics and Plasticity. *Developmental Cell*, **38**, 610-20.

Phair RD, Misteli T (2000) High mobility of proteins in the mammalian cell nucleus. *Nature*, **404**, 604-9.

Phair RD, Misteli T (2001) Kinetic modelling approaches to in vivo imaging. *Nature Reviews Molecular Cell Biology*, **2**, 898-907.

Powrie EA, Ciocanel V, Kreiling JA, Gagnon JA, Sandstede B, Mowry KL (2016) Using in vivo imaging to measure RNA mobility in Xenopus laevis oocytes. *Methods*, **98**, 60-5.

Prasher DC, Eckenrode VK, Ward WW, Prendergast FG, Cormier MJ (1992) Primary structure of the Aequorea victoria green-fluorescent protein. *Gene*, **111**, 229-33.

Presley JF, Cole NB, Schroer TA, Hirschberg K, Zaal KJ, Lippincott-Schwartz J (1997) ER-to-Golgi transport visualized in living cells. *Nature*, **389**, 81-5.

Rafferty KA (1969) Mass culture of amphibian cells: methods and observations concerning stability of cell type. *Biology of Amphibian Tumors. Springer, New York.*

Rankin J, Ellard S (2006) The laminopathies: a clinical review. *Clinical Genetics*, **70**, 261-74.

Rapsomaniki MA, Kotsantis P, Symeonidou IE, Giakoumakis NN, Taraviras S, Lygerou Z (2012) easyFRAP: an interactive, easy-to-use tool for qualitative and quantitative analysis of FRAP data. *Bioinformatics*, **28**, 1800-1.
easyFRAP User Manual: ccl.med.upatras.gr/data/uploads/easyfrap_manual.pdf

Ray-Gallet D, Quivy JP, Scamps C, Martini EM, Lipinski M, Almouzni G (2002) HIRA is critical for a nucleosome assembly pathway independent of DNA synthesis. *Molecular Cell*, **9**, 1091-100.

Ray-Gallet D, Woolfe A, Vassias I, Pellentz C, Lacoste N, Puri A, Schultz DC, Pchelintsev NA, Adams PD, Jansen LE, Almouzni G (2011) Dynamics of histone H3 deposition in vivo reveal a nucleosome gap-filling mechanism for H3.3 to maintain chromatin integrity. *Molecular Cell*, **44**, 928-41.

Ray-Gallet D, Ricketts MD, Sato Y, Gupta K, Boyarchuk E, Senda T, Marmorstein R, Almouzni G (2018) Functional activity of the H3.3 histone chaperone complex HIRA requires trimerization of the HIRAsubunit. *Nature communications*, **9**, 3103.

Ricketts MD, Frederick B, Hoff H, Tang Y, Schultz DC, Singh Rai T, Grazia Vizioli M, Adams PD, Marmorstein R (2015) Ubinuclein-1 confers histone H3.3-specific-binding by the HIRA histone chaperone complex. *Nature Communications*, **6**, 7711.

Risca VI, Greenleaf WJ (2015) Unraveling the 3D genome: genomics tools for multiscale exploration. *Trends in Genetics*, **31**, 357-72.

Rupp RA, Becker PB (2005) Gene regulation by histone H1: new links to DNA methylation. *Cell*, **123**, 1178-9.

Santenard A, Ziegler-Birling C, Koch M, Tora L, Bannister AJ, Torres-Padilla ME (2010) Heterochromatin formation in the mouse embryo requires critical residues of the histone variant H3.3. *Nature Cell Biology*, **12**, 853-62.

Schäpe J, Prausse S, Radmacher M, Stick R (2009) Influence of lamin A on the mechanical properties of amphibian oocyte nuclei measured by atomic force microscopy. *Biophysical Journal*, **96**, 4319-25.

Schneider TD, Arteaga-Salas JM, Mentele E, David R, Nicetto D, Imhof A, Rupp RA (2011) Stage-specific histone modification profiles reveal global transitions in the Xenopus embryonic epigenome. *PLoS One*, **6**, e22548.

Schwartzentruber J, Korshunov A, Liu XY, Jones DT, Pfaff E, Jacob K, Sturm D, Fontebasso AM, Quang DA, Tönjes M et al. (2012) Driver mutations in histone H3.3 and chromatin remodelling genes in paediatric glioblastoma. *Nature*, **482**, 226-31.

Serbus LR, Cha BJ, Theurkauf WE, Saxton WM (2005) Dynein and the actin cytoskeleton control kinesin-driven cytoplasmic streaming in Drosophila oocytes. *Development*, **132**, 3743-52.

Shechter D, Dormann HL, Allis CD, Hake SB (2007) Extraction, purification and analysis of histones. *Nature Protocols*, **2**, 1445-57.

Sitbon D, Podsypanina K, Yadav T, Almouzni G (2017) Shaping Chromatin in the Nucleus: The Bricks and the Architects. *Cold Spring Harbor Symposia on Quantitative Biology*, **82**, 1-14.

Surani MA, Hayashi K, Hajkova P (2007) Genetic and epigenetic regulators of pluripotency. *Cell*, **128**, 747-62.

Suzuki K, Miyazaki M, Takagi J, Itabashi T, Ishiwata S (2017) Spatial confinement of active microtubule networks induces large-scale rotational cytoplasmic flow. *PNAS*, **114**, 2922-7.

Szenker E, Ray-Gallet D, Almouzni G (2011) The double face of the histone variant H3.3. *Cell Research*, **21**, 421-34.

Tagami H, Ray-Gallet D, Almouzni G, Nakatani Y (2004) Histone H3.1 and H3.3 complexes mediate nucleosome assembly pathways dependent or independent of DNA synthesis. *Cell*, **116**, 51-61.

Talbert PB, Henikoff S (2017) Histone variants on the move: substrates for chromatin dynamics. *Nature Reviews Molecular Cell Biology*, **18**, 115-26.

Taniura H, Glass C, Gerace L (1995) A chromatin binding site in the tail domain of nuclear lamins that interacts with core histones. *Journal of Cell Biology*, **131**, 33-44.

Torres-Padilla ME, Bannister AJ, Hurd PJ, Kouzarides T, Zernicka-Goetz M (2006) Dynamic distribution of the replacement histone variant H3.3 in the mouse oocyte and preimplantation embryos. *The International Journal of Developmental Biology*, **50**, 455-61.

Ueda H, Yokota E, Kutsuna N, Shimada T, Tamura K, Shimmen T, Hasezawa S, Dolja VV, Hara-Nishimura I (2010) Myosin-dependent endoplasmic reticulum motility and F-actin organization in plant cells. *PNAS*, **107**, 6894-9.

van Steensel B (2011) Chromatin: constructing the big picture. *EMBO Journal*, **30**, 1885-95.

Weinberger L, Ayyash M, Novershtern N, Hanna JH (2016) Dynamic stem cell states: naive to primed pluripotency in rodents and humans. *Nature Reviews Molecular Cell Biology*, **17**, 155-69.

Wessel D, Flügge UI (1984) A method for the quantitative recovery of protein in dilute solution in the presence of detergents and lipids. *Analytical Biochemistry*, **138**, 141-3.

Wiedemann SM, Mildner SN, Bönisch C, Israel L, Maiser A, Matheisl S, Straub T, Merkl R, Leonhardt H, Kremmer E, Schermelleh L, Hake SB (2010) Identification and characterization of two novel primate-specific histone H3 variants, H3.X and H3.Y. *Journal of Cell Biology*, **190**, 777-91.

Williams PH, Hagemann A, González-Gaitán M, Smith JC (2004) Visualizing long-range movement of the morphogen Xnr2 in the Xenopus embryo. *Current Biology*, **14**, 1916-23.

Woodhouse FG, Goldstein RE (2012) Spontaneous circulation of confined active suspensions. *Physical Review Letters*, **109**, 168105.

Woodhouse FG, Goldstein RE (2013) Cytoplasmic streaming in plant cells emerges naturally by microfilament self-organization. *PNAS*, **110**, 14132-7.

Yadav T, Quivy JP, Almouzni G (2018) Chromatin plasticity: A versatile landscape that underlies cell fate and identity. *Science*, **361**, 1332-6.

Zink LM, Hake SB (2016) Histone variants: nuclear function and disease. *Current Opinion in Genetics & Development*, **37**, 82-9.

Appendix III: R macro: FRAP evaluation for Leica TCS SP5 II

```
// FRAP Evaluation for SP5


//Spot or Half nucleus FRAP

macro "empty   Action tool- C037T4d14 " {
}

macro "FRAP Evaluation SP5   Action Tool - C900T3e161"{

//select a directory


        //dir=getDirectory("Select a Directory for import");
        dir=File.openDialog("Select the Lif file");
        //filenames=getFileList(dir);
        //Array.sort(filenames);

        function list(name, a) {
                  print(name);
                 for (i=0; i<a.length; i++)
                print("   "+a[i]);
        }

        //list("filenames", filenames);

        dir2=getDirectory("Select a Directory for export");
        //dir2=File.openDialog("Select the Lif file");
        //dir2=dir2+"/";  //###windows: change for mac to \
        print(dir2);




        items =newArray("Spot", "Halfnucleus");


//Initial settings

        Dialog.create("Initial settings");
        Dialog.addNumber("Cell to start with:", 1 );
        Dialog.addNumber("Number of prebleach frames:", 20 );
        Dialog.addNumber("Number of bleach frames:", 2 );
        Dialog.addNumber("Total number of cells:", 0 );
        Dialog.addNumber("Diameter of the bleach ROI in pixel:", 30 );
        Dialog.addCheckbox("Zoom in function for bleaching used", false);
        Dialog.addChoice("FRAP", items, items[0]);

        Dialog.show();

        u = Dialog.getNumber();
        prebleach = Dialog.getNumber();
        bleachf = Dialog.getNumber();
        numberofcells = Dialog.getNumber();
        diameter = Dialog.getNumber();
        regok= Dialog.getCheckbox();
        FRAPtype= Dialog.getChoice();

        u=u-1
;



//Zoom in
        if (regok==false) {
                zoomin = "No";
        }
        if (regok==true) {
                zoomin = "Yes";
        }


//count
```

```
	print("Total number of cells",numberofcells);

//Evaluate single cells

	do {
		e=u+1;


//Delete ROIs
		r=roiManager("count");
		if(r >0) {
			roiManager("Deselect");
			roiManager("Delete");
		}


//Import dataset in alphabetic order


		run("Bio-Formats Macro Extensions");

		//path = dir + filenames [u];
		//titlecell=filenames [u];

		run("Bio-Formats Importer", "open=[dir] autoscale color_mode=Default
view=[Standard ImageJ] stack_order=Default series_"+e);


		fulltitle=getTitle();
		indexslash= indexOf(fulltitle, "/");
		print(indexslash);
		titlecell=substring(fulltitle, 0, indexslash);
		print("Name", titlecell);
		//print("Filename", filenames [u]);

		if (nImages>1) {
			selectImage(2);
			close();
		}



		if (isOpen("Exception")) {
			selectWindow("Exception");
			run("Close");
		}

		skip=getBoolean("Would you like to skip this cell?");

		if (skip==true) {
			close();
		}

		else if (skip==false) {

	//Get time interval

			timeinterval= Stack.getFrameInterval();
			//timeinterval=timeinterval*1000;
	//FRAP stack


			frapstack=getImageID();
			setSlice(prebleach);
			resetMinAndMax();



	//Save Prebleach Image



			setSlice(prebleach);
			resetMinAndMax();
			run("Select All");
			run("Copy");
```

```
                run("Internal Clipboard");
                saveAs("Jpeg", dir2 + "Image" + titlecell);
                close();



        //Save FRAP

                saveAs("tiff", dir2 + titlecell);


        //Filter Gaussian Blur

                setSlice(1);
                run("Select None");
                run("Gaussian Blur...", "sigma=2 stack");

        //BleachROI

                if (zoomin =="No") {
                        setSlice(prebleach+1);
                        setAutoThreshold("Default dark");
                        run("Create Selection");
                        roiManager("Add");
                        roiManager("Select", 0);
                        roiManager("Rename", 2);
                }
                if (zoomin =="Yes") {

                        setSlice(prebleach +3);

        //Spot or half nucleus
                        if (FRAPtype ==items[0]){
                                makeOval(100, 100, diameter, diameter);
                                roiManager("Add");
                                roiManager("Select", 0);
                                title = "WaitForUser";
                                msg = "Move the ROI to the bleached area and click
\"OK\".";
                                waitForUser(title, msg);
                                roiManager("Update");
                        }
                        else {
                                makeRectangle(100, 100, 150, 100);
                                roiManager("Add");
                                roiManager("Select", 0);
                                title = "WaitForUser";
                                msg = "Ajust and move the ROI to the bleached area and
click \"OK\".";
                                waitForUser(title, msg);
                                roiManager("Update");
                        }
                        roiManager("Select", 0);
                        roiManager("Rename", 2);

                }


        //Delete Bleach Images

                for (i=0; i<bleachf; i++) {
                        setSlice(prebleach+1);
                        run("Delete Slice");
                }




        //create Image to decide if registration is needed

                selectImage(1);
                setSlice(prebleach);
                run("Select All");
                run("Copy");
                run("Internal Clipboard");
                run("Select None");
```

```
setAutoThreshold("Default dark");
getThreshold(lower, upper);
setThreshold(lower +3, 16383);
run("Create Selection");
roiManager("Add");

selectImage(1);
setSlice(nSlices);
run("Select All");
run("Copy");
run("Internal Clipboard");
setAutoThreshold("Default dark");
getThreshold(lower, upper);
setThreshold(lower +3, 16383);
run("Create Selection");
roiManager("Add");

selectWindow("Clipboard");
close();
selectWindow("Clipboard-1");
close();

newImage("Untitled", "RGB Black", 256, 256, 1);
run("Colors...", "foreground=white background=black  selection=yellow");
roiManager("Select", 1);
roiManager("Draw");
roiManager("Select", 1);
roiManager("Delete");
roiManager("Select", 1);

run("Colors...", "foreground=green background=black  selection=yellow");
roiManager("Draw");
roiManager("Select", 1);
roiManager("Delete");
selectWindow("Untitled");


// Registration?

reg=getBoolean("Does the stack has to be registered?");

if (reg==false) {
	selectWindow("Untitled");
	close();
	registration = "No";
}

if (reg==true) {
	selectWindow("Untitled");
	close();
	registration = "Yes";




	if (FRAPtype ==items[0]) {

		setSlice(1);
		run("StackReg", "transformation=[Rigid Body]");


	}

	else {

		title = "WaitForUser";
		msg = "Set the timepoint at which the recovery is almost
complete and click \"OK\".";
		waitForUser(title, msg);

		splitAt=round(nSlices/2);
		beforereg=getImageID();
		splitAt=getSliceNumber();
		if (splitAt >nSlices) {
			exit("Error: split > nSlices");
		}
```

```
                                        run("Select All");
                                        titleimage=getTitle();
                                        run("Duplicate...", "title="+titleimage+" duplicate");
                                        part1=getImageID();
                                        rename(titleimage + "1-"+splitAt);
                                        run("Duplicate...", "title="+titleimage+" duplicate");
                                        part2=getImageID();
                                        rename(titleimage +splitAt+1+"-"+ nSlices);
                                        for (i=1; i<=splitAt; i++) {
                                                setSlice(1);
                                                run("Delete Slice");
                                        }
                                        selectImage(part1);
                                        for (i=nSlices; i>splitAt; i--) {
                                                setSlice(i);
                                                run("Delete Slice");
                                        }
                                        selectImage(part1);
                                        setSlice(1);
                                        selectImage(part2);
                                        setSlice(1);

                                        //Register second stack



                                        run("StackReg", "transformation=[Rigid Body]");



                                        //Concatenate

                                        selectImage(part1);
                                        rename(1);
                                        selectImage(part2);
                                        rename(2);

                                        run("Concatenate...", "stack1=1 stack2=2
title=Registered");
                                        selectImage("Registered");



                                        regImage=getImageID();
                                        rename("Registered"+titleimage);
                                }



                                saveAs("tiff", dir2 + titlecell +"_registered");



                        }


                        /*if (nImages>1) {
                                selectImage(regImage);



                                title = "WaitForUser";
                                msg = "Check if the registration was successful and click
\"OK\".";
                                waitForUser(title, msg);

                                regok=getBoolean("Was the registration successful? ");

                                if (regok==false) {
                                        selectImage(regImage);
                                        close();
                                        registration = "No";
                                }

                                if (regok==true) {
                                        selectImage(beforereg);
                                        close();
```

```
                        }
                }
                */

        //Select total ROI

                //additional cells?

                selectImage(1);
                resetMinAndMax();
                cell=getBoolean("Does the image contain an additional cell?");
                if (cell==true) {
                        setTool("polygon");
                        title = "WaitForUser";
                        msg = "Outline the area containing the additional cell to be
removed and click \"OK\".";
                        waitForUser(title, msg);

                        roiManager("Add");
                        run("Select None");
                        selectImage(1);
                        cells=getImageID();
                        run("Duplicate...", "title=cell.tif duplicate");
                        roiManager("Select", 1);
                        run("Colors...", "foreground=white background=black
        selection=yellow");
                        run("Clear", "stack");
                        run("Select None");
                        roiManager("Select", 1);
                        roiManager("Delete");
                }


        //Adjust threshold for total ROI

                r=roiManager("count");
                if(r < 1) {
                        exit("You need the ROI of the snapshot. Start from the
beginning.")
                }

                if(r > 1) {
                        title = "WaitForUser";
                        msg = "You have too much ROIs. Delete all ROI's but the
Snapshot-ROI and click \"OK\".";
                        waitForUser(title, msg);
                }


                i=0;

                do {
                //Prebleach ROI

                        cells=getImageID();
                        selectImage(cells);
                        setSlice(prebleach);



                        run("Select All");
                        run("Copy");
                        run("Internal Clipboard");
                        run("Select None");

                        if (i>0) {
                                setThreshold(prelower, preupper);
                        }
                        else {
                                setAutoThreshold("Default dark");
                        }


                        if (lower == 0) {
                                setTool("polygon");
                                resetThreshold();
                                resetMinAndMax();
```

```
                                        title = "WaitForUser";
                                        msg = "Draw total ROI by hand and click \"OK\".";
                                        waitForUser(title, msg);
                                        roiManager("Add");
                                        roiManager("Select", 1);
                                        roiManager("Rename", 1);
                                        roiManager("Sort");
                                        selectWindow("Clipboard");
                                        close();
                                        th = false;
                                        th1 = 0;
                                        th2 = 0;
                                }


                                if(lower > 0) {
                                        run("Create Selection");
                                        roiManager("Add");
                                        if (i>0) {
                                                th1 = prelower;
                                        }
                                        else {
                                                th1 = lower;
                                        }

                                //Last image
                                        selectImage(cells);
                                        setSlice(nSlices);
                                        run("Select All");
                                        run("Copy");
                                        run("Internal Clipboard");
                                        if (i>0) {
                                                setThreshold(lastlower, lastupper);
                                        }
                                        else {
                                                setAutoThreshold("Default dark");
                                        }

                                        if (i>0) {
                                                th2=lastlower;
                                        }
                                        else {
                                                th2= lower;
                                        }

                                        if (lower == 0) {
                                                setTool("polygon");
                                                resetThreshold();
                                                resetMinAndMax();
                                                title = "WaitForUser";
                                                msg = "Draw total ROI by hand and click \"OK\".";
                                                waitForUser(title, msg);
                                                roiManager("Add");
                                                roiManager("Select", 1);
                                                roiManager("Delete");
                                                roiManager("Select", 1);
                                                roiManager("Rename", 1);
                                                roiManager("Sort");
                                                selectWindow("Clipboard");
                                                close();
                                                selectWindow("Clipboard-1");
                                                close();
                                                th = false;
                                        }

                                        if (lower > 0) {
                                                run("Create Selection");
                                                roiManager("Add");
                                                selectWindow("Clipboard");
                                                close();
                                                selectWindow("Clipboard-1");
                                                close();

                                //Create minimal ROI

                                                newImage("Untitled", "8-bit White", 256, 256, 1);
                                                run("Colors...", "foreground=black
background=white      selection=yellow");
```

```
                                        nn=1+i;
                                        mm=2+i;
                                        roiManager("select", newArray(nn,mm));
                                        roiManager("AND");
                                        run("Fill");
                                        run("Select None");

                                        //###Change of automatic ROIis not working
                                        //run("Invert");
                                        run("Fill Holes");
                                        setAutoThreshold("Default");
                                        //setAutoThreshold("Default dark");
                                        run("Create Selection");
                                        roiManager("Add");
                                        selectWindow("Untitled");
                                        close();
                                        roiManager("Deselect");
                                        roiManager("Select", 1 + i);
                                        roiManager("Delete");
                                        roiManager("Select", 1 + i);
                                        roiManager("Delete");
                                        roiManager("Select", 1 + i);
                                        resetThreshold();
                                        setTool("polygon");
                                        run("Select None");
                                        selectImage(cells);
                                        setSlice(prebleach);
                                        roiManager("Select", 1 +i);

                        //check threshold

                                        selectImage(cells);
                                        setSlice(nSlices);
                                        run("Select None");
                                        resetMinAndMax();
                                        roiManager("Select", 1 + i);
                                        i=i+1;
                                        th=getBoolean("Do you want to modify the ROI by
changing the threshold (default: Autothreshold +3)");

                                        if(th==true){
                                                run("Threshold...");
                                                run("Select None");
                                                setSlice(prebleach);
                                                setAutoThreshold("Default dark");
                                                title = "WaitForUser";
                                                msg = "Use the upper\"Threshold\" tool to
adjust the threshold, then click \"OK\".";
                                                waitForUser(title, msg);
                                                getThreshold(lower, upper);
                                                prelower=lower;
                                                preupper=upper;

                                                setSlice(nSlices);
                                                setAutoThreshold("Default dark");
                                                title = "WaitForUser";
                                                msg = "Use the upper\"Threshold\" tool to
adjust the threshold, then click \"OK\".";
                                                waitForUser(title, msg);
                                                getThreshold(lower, upper);
                                                lastlower=lower;
                                                lastupper=upper;
                                        }
                                    }
                                }

                        } while (th == true);


        //Delete dispensable ROIs


                        roiManager("Select", i);
                        roiManager("Rename", 1);
                        roiManager("Sort");
                        while (i > 1) {
                                roiManager("Select", i -2);
                                roiManager("Delete");
```

```
			i=i-1;

		}


		if (nImages>1) {
			selectImage(cells);
			close();
		}


	//Possibility to draw the ROI by hand

		roiManager("Select", 0);
		tROI=getBoolean("Do you want to draw the total ROI by hand?");

		if(tROI==true){

			setTool("polygon");

			roiManager("Select", 0);
			roiManager("Delete");

			setSlice(prebleach);


			title = "WaitForUser";
			msg = "Draw the ROI and click \"OK\".";
			waitForUser(title, msg);



			roiManager("Add");

			roiManager("Select", 1);
			roiManager("Rename", 1);
			roiManager("Sort");
			th1 = 0;
			th2 = 0;
		}

	//background selection

		i=0;
		r=roiManager("count");

		if (r>2) {
			title = "WaitForUser";
			msg = "You have more than two ROI's. Delete additional ROI's and
click \"OK\".";
			waitForUser(title, msg);
		}

		resetMinAndMax();

		//if (snaprotate ==1) {
		//	run("Rotate 90 Degrees Right");
		//}

		//Wrong image size?

		x = getWidth();

		if (x > 256) {
			makeRectangle(128, 128, 256, 256);
			run("Crop");
			resetMinAndMax();
		}

		//Draw background ROI

		title = "WaitForUser";
		msg = "Draw the background ROI and click \"OK\".";
		waitForUser(title, msg);



		roiManager("Add");
```

```
                roiManager("Select", 2);
                roiManager("Rename", 3);
                resetThreshold();
                roiManager("Select",2);
                resetMinAndMax();


        //Create Bleach and unbleach ROI


                if (nImages >1) {
                        print("close all open clipboards");
                }

                run("Colors...", "foreground=black background=white selection=yellow");

                frames=nSlices;
                totalROI = 0;
                bleachROI = 1;
                backgroundROI = 2;


                roiManager("select", newArray(totalROI,bleachROI));
                roiManager("AND");
                roiManager("Add");
                bleachedArea = 3;


                roiManager("select", newArray(totalROI,bleachedArea));
                roiManager("XOR");
                roiManager("Add");
                unbleachedArea = 4;



                resetMinAndMax();
                roiManager("Select", backgroundROI);
                roiManager("Rename", "4");
                roiManager("Select", totalROI);
                roiManager("Rename", "1");
                roiManager("Select", bleachROI);
                roiManager("Rename", "5");
                roiManager("Select", bleachedArea);
                roiManager("Rename", "2");
                roiManager("Select", unbleachedArea);
                roiManager("Rename", "3");
                roiManager("Sort");

                setTool("polygon");
                roiManager("save", dir2 + "RoiSet" + titlecell + ".zip");


        //Profile Plot


        b=256;
                n = nResults;



                run("Set Measurements...", "  mean limit redirect=None decimal=3");
                run("Colors...", "foreground=black background=white selection=yellow");


run("Profile Plot Options...", "width=256 height=256 minimum=0 maximum=0 do vertical
interpolate draw");


        //binary Image

                newImage("Untitled", "RGB Black", 256, 256, 1);
                roiManager("Select", totalROI);
                run("Colors...", "foreground=white background=black selection=yellow");
                run("Fill");
                run("Select None");
                run("Specify...", "width=255 height=256 x=1 y=0");
                run("Crop");
                saveAs("tiff", dir2 + "binary" + titlecell);
```

```
run("Select All");
setKeyDown("alt"); //rotate
profile = getProfile();

//tp prebleach

run("Colors...", "foreground=black background=white selection=yellow");

selectImage(1);
setSlice(prebleach);
run("Select All");
run("Copy");
run("Internal Clipboard");
roiManager("Select", totalROI);
run("Make Inverse");
run("Fill");
run("Select None");
run("Reslice [/]...", "input=1.000 output=1.000 start=Top");
setThreshold(1, 16383);
run("Plot Z-axis Profile");
ppprebleach = newArray(b);
for (i=0; i<b; i++) {
	ppprebleach[i] = getResult('Mean', i);
}

//tp postbleach

run("Colors...", "foreground=black background=white selection=yellow");

selectImage(1);
run("Next Slice [>]");
run("Select All");
run("Copy");
run("Internal Clipboard");
roiManager("Select", totalROI);
run("Make Inverse");
run("Fill");
run("Select None");
run("Reslice [/]...", "input=1.000 output=1.000 start=Top");
setThreshold(1, 16383);
run("Plot Z-axis Profile");

pppostbleach = newArray(b);
for (i=0; i<b; i++) {
	pppostbleach[i] = getResult('Mean', i);
}

//tp last image

run("Colors...", "foreground=black background=white selection=yellow");

selectImage(1);
setSlice(nSlices);
run("Select All");
run("Copy");
run("Internal Clipboard");
roiManager("Select", totalROI);
run("Make Inverse");
run("Fill");
run("Select None");
run("Reslice [/]...", "input=1.000 output=1.000 start=Top");
setThreshold(1, 16383);
run("Plot Z-axis Profile");

pplastframe = newArray(b);

for (i=0; i<b; i++) {
	pplastframe[i] = getResult('Mean', i);
}

//close windows

selectWindow("Reslice of Clipboard");
close();
selectWindow("Reslice of Clipboard-1");
close();
selectWindow("Reslice of Clipboard-2");
close();
```

```
selectWindow("Clipboard");
close();
selectWindow("Clipboard-1");
close();
selectWindow("Clipboard-2");
close();
selectWindow("Reslice of Clipboard-0-0");
close();
selectWindow("Reslice of Clipboard-1-0-0");
close();
selectWindow("Reslice of Clipboard-2-0-0");
close();
selectImage(2);
close();



roiManager("Deselect");


//Measure mean intensity over time

selectImage(1);
roiManager("Select", 0);

run("Plot Z-axis Profile");
aa = newArray(frames);
for (i=0; i<frames; i++) {
	aa[i] = getResult ('Mean', i);
}

roiManager("Deselect");
selectImage(1);
roiManager("Select", 1);

run("Plot Z-axis Profile");
bb = newArray(frames);
for (i=0; i<frames; i++) {
	bb[i] = getResult ('Mean', i);
}

roiManager("Deselect");
selectImage(1);
roiManager("Select", 2);

run("Plot Z-axis Profile");
cc = newArray(frames);
for (i=0; i<frames; i++) {
	cc[i]= getResult ('Mean', i);
}

roiManager("Deselect");
selectImage(1);
roiManager("Select", 3);

run("Plot Z-axis Profile");
dd = newArray(frames);
for (i=0; i<frames; i++) {
	dd[i]= getResult ('Mean', i);
}

ee = newArray(frames);
for (i=0; i<frames; i++) {
	if (i <prebleach +1) {
		ee[i]= 0;
	}
	if (i >= prebleach +1) {
		ee[i]= (i-prebleach)*timeinterval;
	}
}




//print tables
```

```
                        run("Clear Results");

                        run("Select None");
                        for (i=0; i<frames; i++) {
                                setResult("time", i, ee[i]);
                                setResult("total", i, aa[i]);
                                setResult("bleached", i, bb[i]);
                                setResult("unbleached", i, cc[i]);
                                setResult("background", i, dd[i]);
                        }

                        run("Select None");

                        for (i=0; i<b; i++) {
                                setResult("tpprebleach", i, ppprebleach[i]);
                                setResult("tppostbleach", i, pppostbleach[i]);
                                setResult("last frame", i, pplastframe[i]);
                                setResult("pixel per line", i, profile[i]);
                        }



                        selectWindow("Results");
                        close();


                        updateResults();
                        run("Input/Output...", "jpeg=85 gif=-1 file=.csv use_file copy_row
save_column save_row");
                        selectWindow("Results");
                        saveAs("Results", dir2+ titlecell + ".csv");

                        run("Clear Results");



        //Get bleach boundary

                        roiManager("Select", 1);
                        //getSelectionBounds(x, y, width, height);
                        //print(y, height);


                        run("Select None");
                        setResult("number of frames", 0, frames);
                        //setResult("bleach line", 0, bleachborder);
                        setResult("threshold prepbleach", 0, th1);
                        setResult("threshold last frame", 0, th2);
                        setResult("prebleach images", 0, prebleach);
                        setResult("Registration", 0, registration);
                        setResult("Time interval", 0, timeinterval);
                        setResult("FRAP", 0, FRAPtype);




                        updateResults();
                        run("Input/Output...", "jpeg=85 gif=-1 file=.txt use_file copy_row
save_column save_row");
                        selectWindow("Results");
                        saveAs("Results", dir2+ titlecell + ".txt");
                        run("Close");

                        selectImage(2);
                        close();
                        selectImage(2);
                        close();
                        selectImage(2);
                        close();
                        selectImage(1);
                        close();

                } //end of skip cell

        u=u+1;
        print("Done: cell ", u);
        } while (u<numberofcells);
```

<u>Appendix IV:</u> Acknowledgement / Danksagung

„Dankbarkeit ist die Erinnerung des Herzens.“ – *Jean-Baptiste Massillon (1663 – 1742)*

In diesem Sinne danke ich:

Prof. Dr. Ralph Rupp für die Überlassung dieses spannenden und herausfordernden Themas, das in mich gesetzte Vertrauen, die kontinuierliche Unterstützung sowie die vielen wertvollen Hinweise.

Prof. Dr. Peter Becker für die angenehmen Forschungsbedingungen.

Edith Mentele und Barbara Hölscher für die stetige großartige Unterstützung.

Dr. Dario Nicetto, Dr. Gabriele Wagner, Dr. Daniil Pokrovsky, Dr. Alessandro Angerilli, Dr. Ohnmar Hsam, Dr. Stephanie Frenz, Julian Berges und Christian Rößler für die gute Zusammenarbeit.

Dr. Andreas Thomae, Dr. Matthias Hahn und Dr. Tobias Straub für die engagierte Unterstützung bei statistischen und das Confocal betreffenden Fragestellungen.

Mein besonderer Dank gilt Dr. Katrin Schneider für die Programmierung des R-Makros und Herrn Wilfried Fehrle, MD für die Beratung bei sprachlichen Aspekten.

Appendix V: Curriculum vitae

Entfällt aus datenschutzrechtlichen Gründen.